2022

Segmentation of the Wassuk Range Normal Fault System, Nevada (USA): Implications for Earthquake Rupture and Walker Lane Dynamics

Benjamin E. Surpless
Trinity University, bsurples@trinity.edu

Sarah Thorne
Trinity University, sthorne@trinity.edu

Title:

Segmentation of the Wassuk Range normal fault system, Nevada (USA): implications for earthquake rupture and Walker Lane dynamics

Accepted to:

Geological Society of America Bulletin

Authors:

Ben Surpless[1] and Sarah Thorne[1]

[1]Geosciences Department, Trinity University, 1 Trinity Place, San Antonio, TX 78212

E-mail: bsurples@trinity.edu

Keywords: Wassuk Range, seismic hazard, segmentation, bedrock channel profile analysis, remote sensing, fault segment identification

ABSTRACT

Normal faults are commonly segmented along strike, with segments that localize strain and influence propagation of slip during earthquakes. Although geometry of segments can be constrained by fault mapping, it is challenging to determine seismically relevant segments along a fault zone. Because slip histories, geometries, and strength of linkages between normal fault segments fundamentally control the propagation of rupture during earthquakes, and differences in segment slip rates result in differential uplift of adjacent footwalls, we use along-strike changes in footwall morphology to detect fault segments and the relative strength of the mechanical links between them.

We apply a new geomorphic analysis protocol to the Wassuk Range fault, Nevada, within the actively deforming Walker Lane. The protocol examines characteristics of footwall morphology, including range-crest continuity, bedrock-channel long profiles, catchment area variability, and footwall relief, to detect changes in strike-parallel footwall characteristics. Results reveal six domains with significant differences in morphology that we use to identify seismically-relevant fault segments and segment boundaries. We integrate our results with previous studies to determine relative strength of links between the six segments, informing seismic hazard assessment. When combined with recent geodetic studies, our results have implications for the future evolution of the Walker Lane, suggesting changes in the accommodation of strain across the region. Our analysis demonstrates the power of this method to efficiently detect along-strike changes in footwall morphology related to fault behavior, permitting future researchers to perform reconnaissance assessment of normal fault segmentation worldwide.

INTRODUCTION

In seismically-active regions of extension worldwide, major normal faults are commonly segmented along strike, with segments that display different fault slip and seismic histories (e.g., Schwartz and Coppersmith, 1984; dePolo et al., 1991; Stewart and Taylor, 1996; McLeod et al., 2000; Benedetti et al., 2013; Rossi et al., 2017). The distinct segments that make up these faults are commonly separated by geometric discontinuities along strike that localize strain, act as barriers to fault-rupture propagation, and affect the location of earthquake foci (e.g., Segall and Pollard, 1980; Sibson, 1986; Ferrill et al., 1999; Zhang et al., 1999; Soliva and Benedicto, 2004; Manighetti et al., 2015). Thus, the identification of normal fault segments and segment boundaries is critical to better understand seismic hazard analysis in the context of fault system evolution (e.g., Swartz and Coppersmith, 1984; Crone and Haller, 1991; Wesnousky, 2006; 2008; Manighetti et al., 2007; DuRoss et al., 2016; Wong et al., 2016).

In our investigation of the 130-km long Wassuk Range normal fault, western Nevada (Fig. 1), we rely on the first-order control that fault-segment slip histories, geometries, and strengths of linkages between segments place on topographic development of normal fault footwalls (e.g., Ellis et al., 1999; Goldsworthy and Jackson, 2000; Densmore et al., 2004; 2009; Papanikolaou et al., 2013; Rossi et al., 2017; He et al., 2018). Because slope and topographic relief are controlled by erosional denudation of uplifted rock (e.g**.,** Tucker and Bras, 1998; Snyder et al., 2000; Whipple and Tucker, 1999; Whipple, 2004; Boulton and Whittaker, 2009; Boulton et al., 2014) and drainage networks respond to the growth and interaction of fault segments, geomorphic patterns can be used to elucidate the spatial evolution of active, segmented normal fault systems (e.g., Cowie et al., 2006; Boulton and Whittaker, 2009; Papanikolaou et al., 2013).

The Wassuk Range fault zone (Fig. 1), within the actively deforming Walker Lane, is well studied (e.g., Stockli et al., 2002; Krugh, 2008, Surpless, 2010; 2011; Gorynski et al., 2013; Surpless and Kroeger, 2014), so it provides the ideal location to test an integrated set of tools that provides spatial information about fault-system dynamics. We hypothesize that the method described here can identify along-strike changes in footwall character and that these changes can be related to fault segments and the strength of mechanical links between them. We use established methods of bedrock-channel and channel steepness index analysis (e.g., Wobus et al., 2006) to investigate footwall morphology, supplementing these methods with range-crest continuity analysis, catchment area contrasts, and footwall relief analysis to delineate strike-parallel variations in slip rate, fault segmentation, and potential geometric barriers to earthquake rupture.

Our results, when compared to and integrated with geologic studies of the Wassuk Range and published gravity data (Saltus, 1988), provide a clear picture of how normal fault segments interact and may impact the propagation of slip during earthquakes. We also predict how fault segment geometries will accommodate future strain in the context of evolving transtensional Walker Lane dynamics. We demonstrate that this integrated approach is a transferable model that may simplify the initial assessment of seismic hazard along less-well-studied faults worldwide, providing data that permit more targeted and efficient field- and lab-based analyses of active fault systems.

BACKGROUND

Tectonic Setting

The Wassuk Range normal fault is within the Walker Lane – East California shear zone (ECSZ), a complex region of transtension that accommodates approximately 20-25% of dextral strain associated with the North American-Pacific plate boundary and classic Basin and Range extension (e.g., Stewart, 1988; Argus and Gordon, 1991; Bennett et al., 2003; Kreemer et al., 2009; Fig. 1). To the south of the Wassuk Range, the Mina Deflection (MD) (Fig. 1) kinematically links strike-slip deformation of the

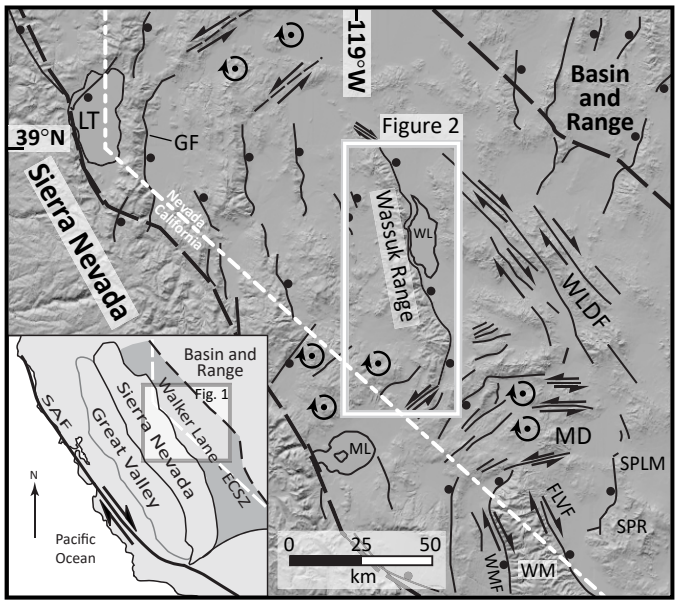

Figure 1. Regional tectonic setting of the Wassuk Range, displaying digital shaded relief, major normal faults, strike-slip faults, and crustal block rotations. Sense of motion is indicated on all faults and positions of block rotations are indicated with a black dot and circle. The region shown in Figure 2 is boxed in white. The bold, black, dashed lines indicate the boundaries of the Walker Lane as delineated by Stewart (1988), and the white dashed line is the California-Nevada state border. Inset displays the important physiographic provinces on the western margin of North America. Abbreviations: ECSZ - East California Shear Zone; FLVF - Fish Lake Valley fault; GF - Genoa fault; LT - Lake Tahoe; MD - Mina deflection; ML - Mono Lake; SAF - San Andreas fault; SPLM - Silver Peak-Lone Mountain extensional complex; SPR - Silver Peak Range; WL - Walker Lake; WLDF - Walker Lane dextral fault complex; WM - White Mountains; and WMF - White Mountains fault. Modified after Stewart (1988); Dilles (1993); Ichinose et al. (1998); Surpless (2008); Lee et al. (2009); Hoeft and Frankel (2010); Carlson et al. (2013); and Surpless and Kroeger (2014).

northern ECSZ (e.g., FLV fault in Fig. 1) to the dextral faults east of the Wassuk Range (WLDF in Fig. 1). The Mina Deflection exhibits clockwise crustal block rotations, normal faults, localized basin formation, and sinistral faults (e.g., Oldow et al., 2001; 2008; Hoeft and Frankel, 2010; Petronis et al., 2007; Busby et al., 2018; DeLano et al., 2019), which in 2020 generated two earthquakes (M5.2 and M6.5) with moment tensors consistent with sinistral displacements (e.g., USGS, 2020a; 2020b; Patton, 2020). The sinistral strike slip fault near the southernmost extent of the Wassuk Range (Figs. 1 and 2) accommodates a portion of this deformation. The position of the right stepover represented by Mina Deflection deformation may be controlled by pre-Paleogene crustal structure (e.g., Oldow et al., 1989; 2008; Burchfiel et al., 1992) and may also explain the partitioning of transtensional strain at ~39°N.

At this latitude, extensional deformation is dominant from the Wassuk Range normal fault to faults of the Lake Tahoe region (LT in Fig. 1; e.g., Surpless et al., 2002; Cashman et al., 2009), and most dextral strain is focused along the Walker Lane dextral faults (WLDF) to the east of the Wassuk Range fault (Fig. 1) (Oldow et al., 2001; 2008; Surpless, 2008). The NW-strike of the WLDF is similar to the Wassuk fault but is at an oblique angle to the dominant NNW strike of the Wassuk fault zone (Figs. 1 and 2).

Geology of the Wassuk Range

Pre-Cenozoic basement rocks in the Wassuk Range consist of Triassic to Jurassic (?) metavolcanic and metasedimentary rocks (Mm in Fig. 2) intruded by Jurassic and Cretaceous plutonic rocks (e.g., Bingler, 1978; Surpless, 2010; 2011; Gorynski et al., 2013). These plutonic rocks (KJg in Fig. 2) formed during Jurassic and Cretaceous Sierran arc magmatism and were part of the Sierra Nevada batholith prior to Basin and Range extension (e.g., Bingler, 1978; Burchfield et al., 1992; Surpless et al., 2002; Surpless, 2011). These plutonic units are predominantly quartz monzonite or similar in composition and exhibit trace-element signatures associated with subduction-related plutonic rocks (e.g., Surpless, 2010; 2011).

The Paleogene unconformity, which truncates Pre-Cenozoic basement rocks, developed during Late Cretaceous-early Paleogene uplift and erosion and was likely caused by some combination of crustal thickening during Sierran magmatism and contractional deformation associated with the Sevier orogeny (e.g., Wernicke, 1992). This period of post-Cretaceous uplift continued until the eruption of Oligocene rhyolite ash-flow tuffs, best exposed in the northern Wassuk Range (e.g., Bingler, 1978; Dilles, 1993; Surpless, 2011; Tt in Fig. 2). After another cessation of magmatism, from ca. 25 Ma until ~15 Ma, the ~15 Ma Lincoln Flat andesite (Tlf in Fig. 2) erupted, immediately preceding the onset of rapid extension and footwall exhumation in the Wassuk Range (e.g., Stockli et al., 2002; Surpless et al., 2002; Surpless, 2011). This period of large-magnitude, east-west-oriented extension was focused between approximately 15 and 12 Ma and was accommodated by a series of east-dipping normal faults, resulting in westward tilting of fault blocks along the Wassuk Range, so that most preserved Miocene volcanic rocks display westward dips on the west flank of the Wassuk Range (Fig. 2) (e.g., Stockli et al., 2002; Surpless, 2010; 2011; Gorynski et al., 2013).

From ~12 Ma until ~ 4 Ma, footwall cooling and uplift related to extension occurred at a much lower rate (Stockli et al., 2002), accommodated by faults that now dip west at moderate angles (25 – 40°). The earliest Tertiary Wassuk Group (Twg in Fig. 2) sediments were deposited at the beginning of this period, with sedimentation that continued until approximately 7 Ma (e.g., Gilbert and Reynolds, 1973; McIntyre, 1990; Surpless, 2011); these sediments are best-preserved on the west flank of the Wassuk Range (Fig. 2). Interestingly, most Wassuk Group deposition, focused between ~9 Ma and ~7 Ma (McIntyre, 1990), was likely coeval with dextral motion along the Penrod Canyon fault (PCF in Fig. 2) and the Buck Brush Spring fault (BBSF in Fig. 2) (McIntyre, 1990; Surpless, 2011). These faults display no evidence of dextral slip after ca. 7 Ma (McIntyre, 1990; Dilles, 1993). Importantly, Surpless (2011) suggested a clockwise rotation in the minimum compressive stress direction from the Miocene to the present. Palinspastic restoration of Miocene deformation at the latitude of Bald Mountain revealed an

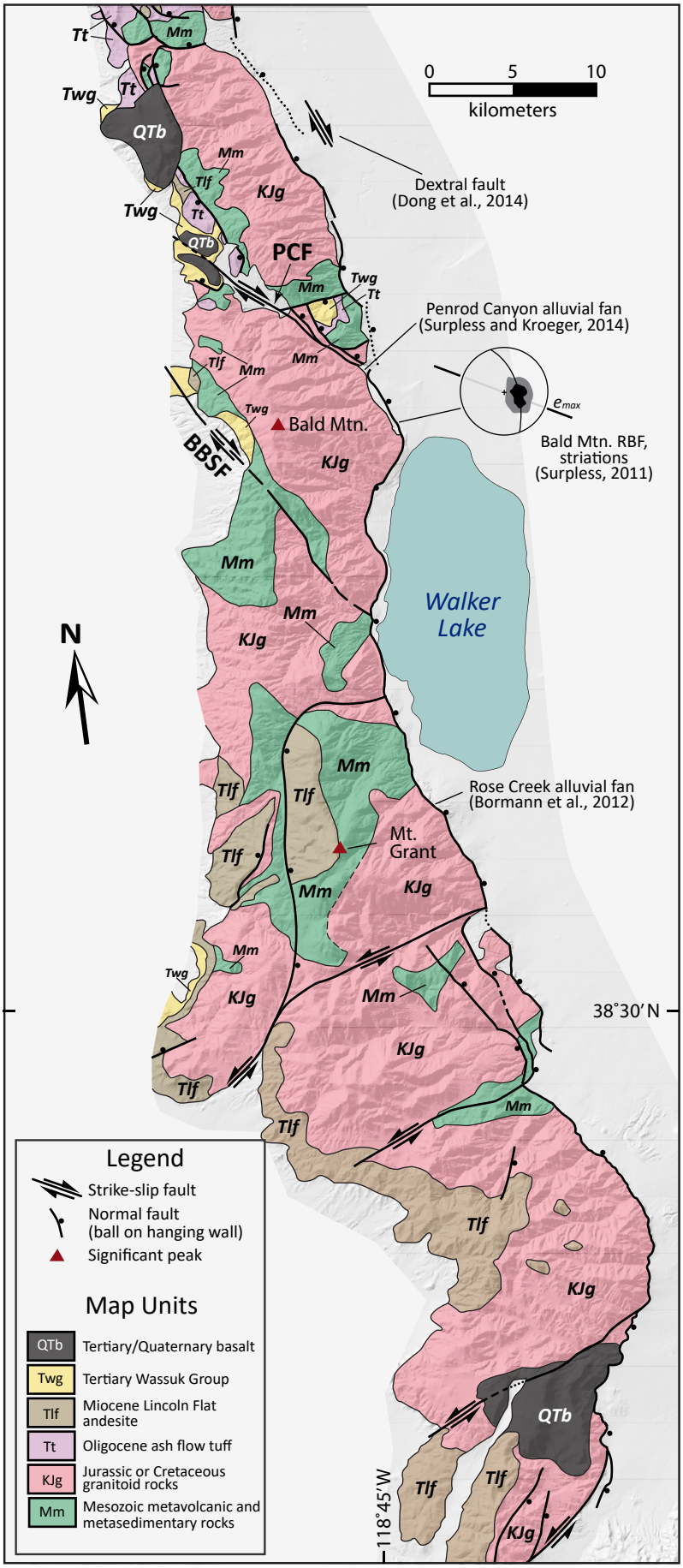

Figure 2. Geologic map of the Wassuk Range. Distribution of map units and faults based on Bingler (1978), Stewart et al. (1981), Klinger (2005), Surpless (2010), Gorynski et al. (2013), and Dong et al. (2014). Abbreviations: BBSF = Buck Brush Springs fault; and PCF = Penrod Canyon fault. Dong et al. (2014) mapped a dextral strike-slip fault outboard of the Shurz range-bounding fault. Surpless (2011) presented detailed fault plane and fault striation measurements along the northern segment of the Bald Mountain range-bounding fault. The best-fit fault plane and contoured striation data are displayed on an equal-area, lower-hemisphere stereonet with a 2σ Kamb contour interval and estimated maximum extension orientation (emax) based on those data (modified from Surpless, 2011). Bormann et al. (2012) presented paleoseismic data documenting past earthquake events at the Rose Creek alluvial fan, and Surpless and Kroeger (2014) documented slip rates at the Penrod Canyon alluvial fan.

approximate E-W to ENE-WSW maximum extensional strain, but structural analysis of the range front fault east of Bald Mountain suggests a recent to modern maximum extensional strain orientation of approximately NW-SE (stereonet data, Fig. 2).

The modern Wassuk Range fault

The active, high-angle, east-dipping Wassuk normal fault (Fig. 1) is dominated by right-stepping, *en echelon* segments (e.g., Demsey, 1987; Wesnousky, 2005) and has slipped at high rates since approximately 4 Ma, with thermochronologic and geologic data suggesting between 2 and 3 km of footwall exhumation since ~4 Ma (Stockli et al., 2002; Krugh, 2008; Gorynski et al., 2013). From ca. 4 Ma to the present, the Wassuk Range normal fault has accommodated rates of slip up to 1.1 mm/yr (Surpless and Kroeger, 2014 *and references therein*) and has one of the highest Holocene slip rates in the Basin and Range Province (dePolo and Anderson, 2000; Wesnousky, 2005). The Wassuk fault displays maximum footwall relief centered on Mt. Grant with decreasing relief along strike to the north and south, approaching zero at the north and south ends of the fault (e.g., Stockli et al., 2002; Krugh, 2008; Gorynski et al., 2013; Surpless and Kroeger, 2014).

Previous researchers have divided the footwall of the Wassuk fault into structural blocks with different magnitudes of fault slip and horizontal axis rotation (Krugh, 2008; Gorynski et al., 2013); faults at high angles (in map view) to the range front fault system (Fig. 2) may act as accommodation zones that permit significantly different magnitudes of slip and horizontal axis rotations between adjacent fault blocks (McIntyre, 1990; Dilles, 1993; Surpless, 2010; 2011; Gorynski et al., 2013). Both Krugh (2008) and Gorynski et al. (2013) suggest that spatial and temporal variations in the accommodation of strain along the Wassuk fault may relate to fault segmentation.

Demsey (1987) and Bormann et al. (2012) used trenching, soil development, and fault scarp morphology to constrain Holocene activity along the Wassuk Range fault system. Demsey (1987) suggests that two major earthquakes, with 2-3 meters offset per event, affected different segments of the fault system. A ca. 4500 yr B.P. earthquake ruptured ~30 km of the southern fault system and a ca. 2500 yr B.P. earthquake ruptured ~50 km of the range front, with rupture that extended to, but not to the north of, the Penrod Canyon fault (PCF in Fig. 2). Based on trench-based analysis of the Rose Creek alluvial fan (Fig. 2), Bormann et al. (2012) established that at least three earthquakes have occurred since ca. 9400 yr B.P., with the most recent event postdating ca. 2810 yr B.P. These events generated ~7.0 m vertical offset, suggesting a Holocene vertical displacement rate of 0.7 ± 0.1 mm/yr slip rate (Bormann et al., 2012). Surpless and Kroeger (2014) used a variety of methods to determine rates of slip similar to those established by Bormann et al. (2012), with a vertical displacement of ~1.1 mm/yr for the southern Wassuk Range, proximal to Mt. Grant, and a vertical slip rate of <0.8 mm/yr further to the north (Fig. 2).

Fault segmentation

The fault growth process exerts a fundamental control on the along-strike segmentation of fault systems, which impacts stress distribution on fault planes and resulting earthquake dynamics (e.g., Field et al., 2014; Wong et al., 2016; 2017). Fault segments along a normal fault zone may interact differently with adjacent segments, with interactions that depend upon the strength of mechanical links between them (Fig. 3). Young, immature fault systems display “soft” connections between segments (e.g., Walsh and Watterson, 1991; Trudgill and Cartwright, 1994; Mansfield and Cartwright, 2001), resulting in a discontinuous fault system (e.g., Manighetti et al., 2015) with relatively independent segments (Fig. 3A). As a fault matures, its segments become mechanically linked, or “hard” linked, resulting in a more continuous fault system with fewer segments (e.g., Walsh and Watterson, 1991; Trudgill and Cartwright, 1994; Manigehtti et al., 2007; 2009; 2015).

Identification of seismically-relevant segments and the discontinuities between those segments remains challenging. Although the zones between segments should display significant cumulative displacement deficits early in fault system evolution (e.g., Ellis and Dunlap, 1988; Peacock, 1991; Soliva

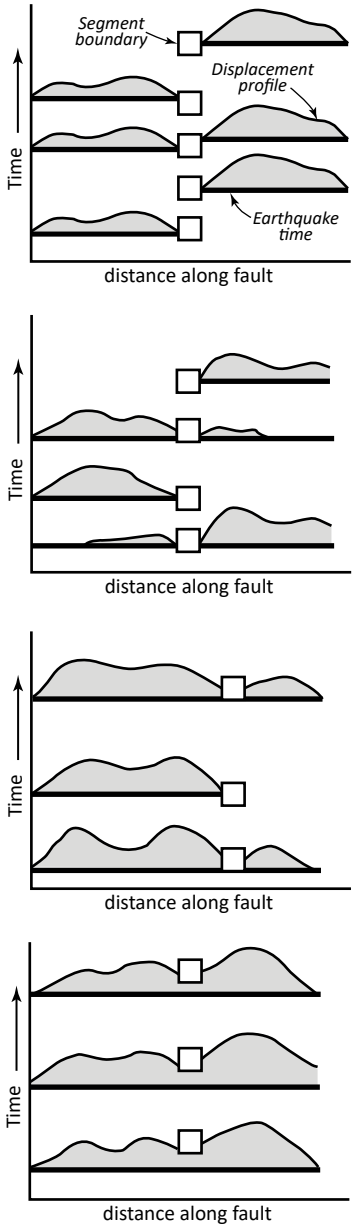

A. INDEPENDENT
Segment boundary is barrier to propagation from either direction. However, adjacent segments may rupture together within uncertainties of timing data.

B. OVERLAP/TRIGGERED SLIP
Segment boundary is commonly barrier to propagation from either direction but rupture propagates past boundary. Post-rupture stress field change may trigger later slip on adjacent segment.

C. MASTER VS. SUBSEGMENT
One segment (on right in diagram) may be dependent on adjacent (master) segment. Dependent segment may be too short to independently generate earthquakes.

D. MULTI-SEGMENT
Segments are mechanically linked (hard linked), but segment boundary remains barrier to propagation, so is at a relative displacement low along the fault-parallel slip profile.

Figure 3. Models for segment interactions along normal faults. Interactions between adjacent segments may change over time if adjacent segments become more strongly mechanically-linked as the fault system matures, thus displaying less segment independence. Note that displacement profiles on adjacent segments consistently display different slip profiles over time, so that long-term slip should produce different magnitudes of footwall uplift. Adapted from Wong et al. (2016).

and Benedicto, 2004), displacement data with enough detail to identify individual segments is difficult to obtain (e.g., DuRoss et al., 2016). This is especially true as a fault system matures; as a fault accumulates more displacement, along-strike variability decreases, making identification of segments based on those data difficult (e.g., Wesnousky, 1988; Sagy et al., 2007; de Joussineau and Aydin, 2009; Manighetti et al., 2015). Researchers have used mapped fault trace geometries (e.g., Wesnousky, 2006; 2008; Manighetti et al., 2015 *and references therein*; Wong et al., 2016), but adjacent segments identified in this way may behave as a single fault due to a mechanical connection between them (e.g., Willemse et al., 1996; Ferrill et al., 1999). Alternatively, seismic-hazard studies have used earthquake rupture initiation and termination data from historic seismicity or paleoseismic studies to define segments (e.g., Wesnousky, 2006; 2008; DuRoss et al., 2016 *and references therein;* Wong et al., 2016; 2017), but these data are rarely available with high enough density along the length of a fault zone to define meaningful fault segment interactions.

Past studies of fault systems worldwide (e.g., Klinger et al., 2011; Hecker et al., 2013 *and references therein*) suggest that the lateral extent of repeated ruptures along a fault segment in the shallow crust are commonly similar over long time scales. This implies that fault zone segment geometries control the length of many ruptures, with some segment boundaries acting as persistent barriers to rupture propagation over many earthquake cycles (e.g., Aki, 1979; Elliott et al., 2015). In addition, strongly segmented earthquake rupture patterns may be more pronounced and persistent on normal faults relative to strike-slip faults (e.g., Biasi and Weldon, 2009; Schwartz et al., 2012; Benedetti et al., 2013; Scharer et al., 2014; Wong et al., 2016). In the absence of sufficient paleoseismic and historical data, the topographic development of the Wassuk Range itself, the footwall of the fault system, records along-strike variability in fault slip that we can relate to the mechanical interaction of segments along fault strike.

Recent studies have demonstrated that patterns in rock uplift are correlated with patterns of topographic metrics for a given climate and lithology (e.g., Kirby and Whipple, 2001; Wobus et al., 2003; 2006; Densmore et al., 2004; Harkins et al., 2007; Cyr and Granger, 2008; Whittaker, 2012; Boulton et al., 2014; Godard et al., 2014; Rossi et al., 2017). A mature normal fault footwall with mechanically-linked segments is expected to exhibit a relatively simple along-strike pattern, with greatest uplift near the central portion of the fault and a smooth decrease in uplift with increasing along-strike distance from that maximum (e.g., Cowie and Scholz, 1992; Dawers et al., 1993; Dawers and Anders, 1995). However, if segments and their boundaries continue to play a fundamental role in rock uplift, with differences in uplift for adjacent along-strike segments, we would expect to see those differences recorded by abrupt along-strike changes in the geomorphic expression of fault-related uplift.

APPROACH AND METHODS

Previous researchers have developed geomorphic analysis methods to detect regions of high rock-uplift rates related to faulting, consistent with the general understanding that bedrock-channel networks will adjust to vertical displacements in active, mountainous regions (e.g., Whipple, 2004; Burbank and Anderson, 2012). Investigation of bedrock channel profiles permits analysis of the rates of rock uplift, fault evolution, and seismic hazard in active orogens (e.g., Kirby et al., 2000; 2003; Wobus et al., 2006; Wei et al., 2015).

In this study, we integrated geologic information with analysis of a digital elevation model (DEM) of the Wassuk Range to qualitatively and quantitatively characterize the geomorphic expression of the footwall of the east-dipping fault in the context of fault system evolution. We extracted longitudinal channel profiles based on a 1/3 arc-s DEM with a ~10 m ground resolution (e.g., USGS, 2017) in combination with GIS software (ArcGIS 10.3.1), the *Stream Profiler* tool, and MATLAB codes as outlined in Whipple et al. (2007). In our analysis, we also extracted map-view catchment and drainage divide data using standard ArcGIS tools.

Longitudinal profiling analysis relies on simple models of river behavior (e.g., Whipple and Tucker, 2002), which predict power law relationships between local channel slopes (S) and upstream drainage area (A) in the form (Eq. 1):

$$S = k_s A^{-\theta} \quad (1)$$

where the steepness index (k_s) and concavity index (θ) can be derived from regression of slope and area data derived from the DEM (e.g., Wobus et al., 2006; Boulton et al., 2014). This stream profiling analysis relies on the fact that although concavity (θ) varies among channels, it typically varies between 0.4 and 0.7 (e.g., Whipple, 2004; Burbank and Anderson, 2012). In order to compare different channels, we use the normalized steepness index, k_{sn}, which is calculated by using a reference concavity (θ_{ref}) of 0.45 for all channels analyzed, a value used in similar studies (e.g., Wobus et al., 2006; DiBiase et al., 2009; Miller et al., 2012; Boulton et al., 2014). Importantly, differences in k_{sn} values do not depend on the chosen reference concavity value (e.g., Wobus et al., 2006).

We extracted all major channel profiles with outlets along the east-dipping, range-bounding normal fault on the western margin of the Walker Lake basin (Fig. 4). We use these data to quantify and describe channel steepness characteristics (k_{sn}), profile shape, horizontal profile length, total change in elevation (relief), and watershed area from the range-crest to the range-bounding fault. Prior to profile analysis and interpretation, we eliminated channels that: 1) are tributaries of the main trunk channel of the watershed; and 2) do not originate where the range crest is clearly-defined (see below). We thus focus on 24 longitudinal profiles (Figs. 4 and 5) to best characterize crest-to-fault morphology to detect strike-parallel changes in channel-profile character.

We define the range crest in relation to the east-dipping range-front fault; the crest coincides with the local drainage divide and is the highest elevation as measured along a fault-perpendicular cross-sectional profile of the range. Where clearly defined, the crest elevations change only gradually subparallel to fault strike, and the steepest slopes away from the range crest are perpendicular to fault strike (to the east or west, in this case). We consider the range crest poorly defined where the along-strike elevation of the crest decreases significantly, so that the steepest slope is no longer toward the fault *or* that the map-view trace of the drainage divide no longer parallels the strike of the range-front fault and displays a more sinuous map-view trace. We consider bedrock trunk channels that originate at the range crest to best represent morphology of the normal fault footwall. The northernmost and southernmost bedrock channel profiles shown in Figure 4 drain from the approximate northern and southern terminations of the Wassuk range crest.

We also analyze the sinuosity of bedrock channels using the sinuosity index, which is quantified by the ratio of the along-channel distance to the shortest map-view path length (e.g., Leopold et al., 1964; Zamolyi et al., 2010). Because sinuosity is scale sensitive (e.g., Lancaster and Bras, 2002), primarily dependent upon the spatial resolution of the analysis (constrained in this study by the 10 m resolution of the DEM), we only consider our bedrock channel sinuosity values relative to each other and not to values from other studies.

Bedrock channels in steady state (where erosion rate is equal to uplift) exhibit unperturbed, concave-up profiles, without breaks in slope or convex-up sections (e.g., Wobus et al., 2006). Channel profiles that display convex sections commonly indicate a channel undergoing a transient response, where the perturbation, or knickpoint, migrates upstream over time (e.g., Hasbargen and Paola, 2000; Crosby and Whipple, 2006; Castillo et al., 2013). These knickpoints may develop due to a range of factors, including, but not limited to, base-level change caused by tectonic factors, debris flows, sediment input from hill slopes, variations in lithology, the presence of faults, or climate fluctuations (e.g., Burbank and Anderson, 2012). Thus, we documented any prominent perturbations in a profile's concave-up shape, including convex sections (e.g., Whittaker et al., 2008; Boulton et al., 2009), and smaller perturbations, or knickpoints, where the simple concave-up profile is interrupted by a break in slope (e.g., Wobus et al., 2006; Kirby and Whipple, 2012). In our analysis of normalized channel

steepness (k_{sn}), we focus on k_{sn} values for the reach closest to the fault for each channel, assuming that these reaches best represent modern footwall uplift rates (e.g., Rossi et al., 2017). All bedrock channel data are included in Table 1.

In addition to comparing along-strike populations of bedrock channels for most geomorphic indices, we also compare populations using a measure that takes into account both topographic relief and channel length. Because profile length values (ranging from 4,250-10,780 m, with an outlier at 23,890 m; Table 1) are so much larger than relief values (ranging from 661-2,097 m; Table 1), analysis that did not account for the difference in scale would be weighted heavily toward differences in long-profile channel length. Thus, we scale each measure (relief and channel length) so that values range from 1.00 to 10.00. In the case of length, we use 10,780 m as our 10.0 value, so that length values are not artificially compressed due to the outlier channel length (channel 19). We use these scaled x (length) and y (relief) values to derive a single value that represents the distance of each channel from the range crest to the outlet, taking both horizontal and vertical change into account. We calculate this value (Z) using the equation (Eq. 3) shown below, which is the equivalent of the length of the hypotenuse in a right triangle:

$$Z = \sqrt{(scaled\ length)^2 + (scaled\ relief)^2} \qquad (3)$$

Once we determined strike-parallel changes in geomorphic indices that we consider indicative of different long-term slip behaviors associated with fault segmentation, we tested the statistical differences between data from adjacent footwall-block domains using T-test analyses of domain population data. The T-test permits evaluation of the mean value of a given measure for two footwall block populations relative to the variability of each population. If the difference between the mean values for each block is large relative to the variabilities for each population, the t-value will exceed 95% confidence, suggesting that the difference in means is statistically significant. If the calculated t value falls below the 95% confidence value, the variability of the populations is too large to demonstrate a statistically significant difference between populations. Exceedance values (from a statistical t-value table) are based on the number of degrees of freedom (n – 2, where n = total number of values in both populations) and probability (P=0.05 or 95% confidence). The t-value calculation (Eq. 2) for the comparison of two populations, 1 and 2, is shown below:

$$t = \frac{\bar{X}_1 - \bar{X}_2}{\sqrt{\frac{var_1}{n_1} + \frac{var_2}{n_2}}} \qquad (2)$$

Where $\bar{X}_1$ is the mean of population 1, var_1 is the variance of population 1 (variance = square of standard deviation), and n_1 is the total number of values in population 1. The denominator of the formula is also known as the standard error of difference of means. Raw T-test result data are included in Table S1, and confidence values based on those T-values are included in Table 2.

DATA AND RESULTS

Range crest continuity and geomorphic analysis

Prior to other analyses, we defined the range crest along the Wassuk Range, subparallel to the range-bounding normal fault. We used the protocol described in **Approach and Methods** to define traces of the range crest (thick gray dotted lines in Fig. 4). The range crest is not continuous or well-defined along the entire length of the Wassuk Range, with 5 map-view discontinuities along strike (Fig. 4). These discontinuities include: a ~5 km right step between the range crest near Bald Mountain relative to the range crest north of the Penrod Canyon fault (Figs. 2 and 4); a ~4 km left step between the Mt. Grant range crest and the Bald Mountain range crest; a ~7 km right step between the range crest at approximately 38°30’ N and the Mt. Grant range crest; and a ~5 km left step between range crests near the southernmost topographic expression of the Wassuk Range (Fig. 4). We only performed detailed geomorphic analysis of the 24 bedrock channels that drain from these range crests (numbered

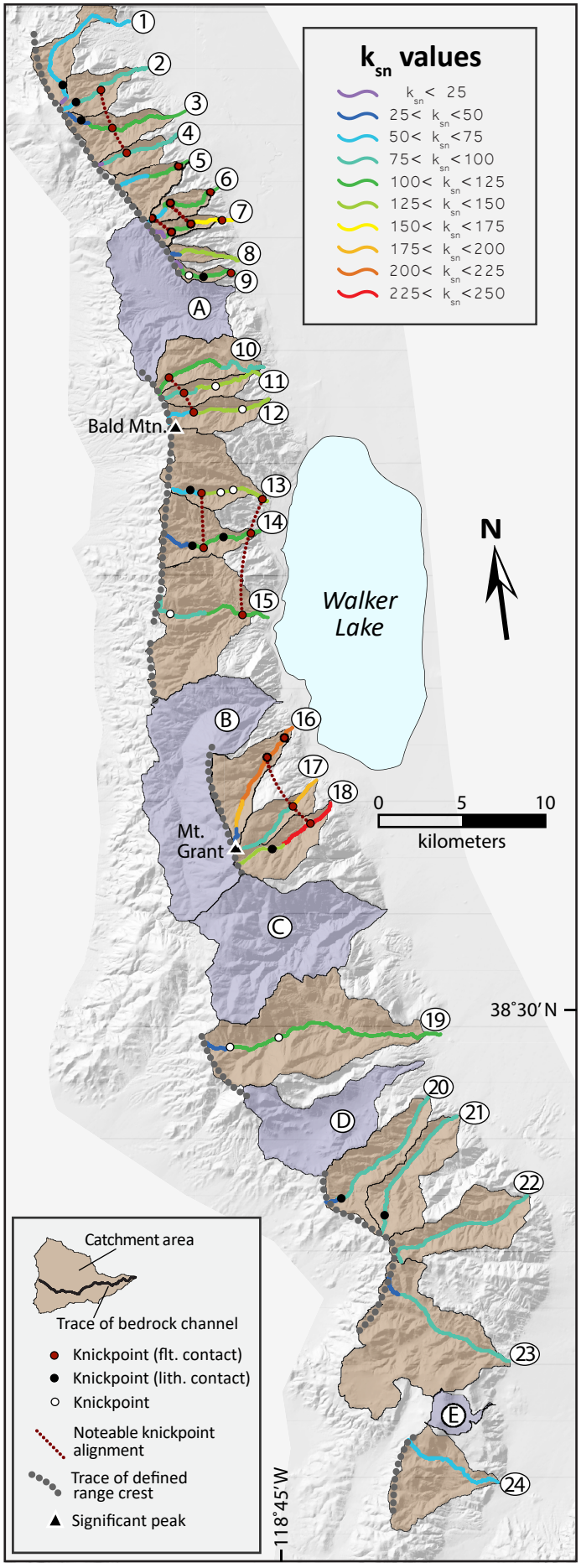

Figure 4. Distribution of catchment areas and bedrock channels with outlets proximal to the Wassuk Range normal fault. Channels are limited to those that are trunk streams originating at a well-defined range crest. Channels are color-coded according to normalized steepness (ksn) value. Watersheds of outlets that drain areas without a well-defined range crest are indicated by letters, and watersheds that drain areas with a well-defined range crest are associated with bedrock channels 1 - 24. See Figure 5 for long-channel profiles for each bedrock channel.

TABLE 1. BEDROCK CHANNEL DATA

Bedrock Channel/Catchment	Along-strike position* (km)	Outlet elev. (m)	Max. elev. (m)	Relief (m)	Channel length (km)	Straight-line distance** (km)	Sinuosity	Aveerage slope (deg.)	Catchment Area (km^2)	Z value for scaled relief-length***	Outlet-reach k_{sn} ($\pm 2\sigma$)	Outlet-reach concavity ($\pm 2\sigma$)	Knickpoint elev. (m)[t]
1	8.0	1324	2370	1046	10.71	5.98	1.79	5.58	8.95	10	72.1 (± 3.0)	0.25 (±0.03)	***2060***
2	10.7	1319	2507	1188	7.73	5.33	1.45	8.74	6.95	7.22	92.5 (±1.9)	0.42 (±0.07)	1760, 2250
3	13.7	1313	2484	1171	9.60	6.06	1.58	6.95	9.41	9.37	100.9 (±2.3)	0.58 (±0.08)	1740, ***2190***
4	14.9	1318	2336	1018	8.22	4.68	1.76	7.06	4.97	7.24	97.7 (±2.9)	0.30 (±0.09)	1910
5	16.5	1292	2267	975	6.86	3.59	1.91	8.09	6.91	5.47	101.9 (±2.0)	0.63 (±0.13)	1410
6	18.7	1296	2517	1221	6.87	4.35	1.58	10.08	4.11	6.45	109.3 (±2.9)	0.46 (±0.14)	1390, 1830, 2410
7	20.6	1280	2486	1206	5.86	4.65	1.26	11.63	3.40	5.46	163.8 (±8.7)	2.40 (±0.36)	1410, 1900, 2180
8	22.9	1302	2436	1134	4.25	3.91	1.09	14.94	2.28	4.09	128.1 (±1.7)	0.37 (±0.08)	-
9	23.6	1289	2397	1108	4.79	3.60	1.33	13.02	1.98	4.18	115.3 (±5.3)	0.10 (±0.09)	1350, ***1810,*** 2020
A	24.4	1353	-	-	-	-	-	-	33.00		-	-	
10	29.1	1343	2840	1497	9.10	6.27	1.45	9.34	12.03	9.90	101.1 (±2.7)	0.73 (±0.10)	2430
11	29.6	1338	2866	1528	8.00	5.66	1.41	10.81	5.25	8.91	130.6 (±7.6)	1.02 (±0.41)	1810, 2230
12	31.0	1344	2838	1494	8.58	5.84	1.47	9.88	7.95	9.34	148.3 (±4.6)	0.95 (±0.14)	1660, 2400
13	38.0	1305	2541	1236	6.81	5.52	1.23	10.29	15.37	6.46	145.0 (±3.3)	0.40 (±0.09)	1370, 1650, 1800, 2030, ***2200***
14	39.7	1304	2374	1070	7.46	5.69	1.31	8.16	12.50	6.49	121.4 (±5.9)	0.10 (±0.12)	1480, 1640, 2030, ***2200***
15	44.9	1308	2414	1106	8.00	6.45	1.24	7.87	30.16	7.24	117.1 (±3.1)	0.48 (±0.15)	1480, 2070
B	49.8	1317	-	-	-	-	-	-	55.87		-	-	
16	51.7	1299	3347	2048	8.74	6.81	1.28	13.19	12.71	12.07	219.9 (±1.0)	0.38 (±0.07)	1520, 1830
17	54.8	1326	3413	2087	7.82	6.13	1.28	14.94	6.68	11.57	190.5 (±9.0)	3.29 (±0.54)	2000
18	56.4	1330	3427	2097	9.37	6.49	1.44	12.61	10.46	12.84	220.4 (±3.6)	0.68 (±0.22)	1800, ***2410***
C	63.0	1391	-	-	-	-	-	-	49.51		-	-	
19	70.7	1378	3029	1651	23.89	13.31	1.79	3.95	43.78	28.98	120.6 (±2.1)	0.64 (±0.22)	2160, 2700
D	72.4	1565	-	-	-	-	-	-	27.68		-	-	
20	74.5	1661	2556	895	10.78	8.29	1.30	4.75	17.06	10.30	87.9 (±1.3)	0.30 (±0.06)	2230
21	76.5	1706	2848	1142	10.29	7.68	1.34	6.33	15.97	10.15	81.9 (±1.0)	0.59 (±0.12)	***2560***
22	82.5	1825	2866	1041	9.84	8.09	1.22	6.04	17.92	9.34	88.4 (±2.6)	0.29 (±0.08)	-
23	93.1	1907	2677	770	9.74	8.60	1.13	4.52	42.37	8.73	93.8 (±4.6)	0.18 (±0.08)	-
E	95.4	1872	-	-	-	-	-	-	4.02		-	-	
24	99.9	1935	2596	661	7.16	5.59	1.28	5.27	18.12	5.11	61.0 (±3.0)	0.28 (±0.03)	-

**Relative to the northernmost topographic expression of the Wassuk Range*

***Straight-line map-view distance from outlet location to range-crest*

****See discussion of Z value in Approach and Methods*

[t] *For convex reaches, the knickpoint elevation is the base of the convex reach. Bold-faced, italic values indicate lithologic contact (Figs. 2-4).*

bedrock channels in Fig. 4). However, as described below, we defined five more catchments along the range in order to both delineate the drainage divide as well as to aid our footwall domain analysis (lettered catchments A – E in Fig. 4).

Long-profile bedrock channel relief, length, shape, and defining footwall domains

From bedrock channel 1 to bedrock channel 9 (Fig. 4), channel relief is fairly constant at approximately 1000-1200 m, but the channel length and map-view distance between the range crest and the range-bounding fault decrease from north to south (Fig. 5; Table 1), resulting in an increase in average slope from a minimum near 5.5° in the north to a maximum of nearly 15.0° in the south (Table 1). Bedrock channel 10 displays higher relief, at about 1500 m, and an increase in length, from the 4.8 km length of channel 9 to the 9.1 km length of channel 10 (Fig. 5; Table 1). Channels 10-12 all display similar shapes, relief, and lengths, suggesting a fundamental change in profile character between channels 9 and 10, a change that coincides with the northernmost range-crest discontinuity described above (Fig. 4).

Further south (Fig. 4), bedrock channels 13-15 all display lower relief (~1100 -1200 m) and shorter lengths (6.8 – 8.0 km) than channels 10-12 (8.0 – 9.1 m), but the general shape of channel profiles 10-15 is similar (Fig. 5; Table 1). The changes in relief and channel length between channels 12 and 13 coincide with a change in strike of the range-bounding fault system near the northern extent of Walker Lake (Figs. 2 and 4). We consider the changes in these measures to be sufficient to analyze channels 10-12 separately from channels 13-15, but there is no associated discontinuity in the range crest (Fig. 4).

In contrast, the abrupt changes in channel profile relief, length, and/or shape that occur between channels 15 and 16, between channels 18 and 19, between channels 19 and 20, and between channels 23 and 24 (Fig. 5; Table 1) coincide with range-crest discontinuities (Fig. 4). Based on differences in along-strike channel profile character, we tentatively divide the Wassuk Range footwall into domains that aid further analysis and discussion. In Figure 6, we display all 24 profiles, divided according to 6 tentative footwall domains, titled, from north to south, Shurz, Bald Mountain, Mt. Grant, Coryville, Luckyboy, and Anchorite Hills, where possible using the same titles suggested by previous researchers (Krugh, 2008; Gorynski et al., 2013). We subdivide the Shurz and Bald Mountain domains into North and South subdomains based on differences in long-channel profiles (Fig. 6) and on differences in geomorphic indices (Table 1) analyzed as part of this study.

Channel profiles to the south of the Mt. Grant domain (channels 19-24) display fundamentally different shapes than profile shapes to the north (Figs 4-6). To the north, profiles display steeper average slopes, with the steepest slopes located near the upper reaches of each profile, and a clear concave-up shape along most of each profile (Figs. 4-6). In contrast, to the south of the Mt. Grant domain, most profiles display a relatively steep initial slope near the upper-reach of each profile that abruptly shallows only a short horizontal distance (commonly 2 – 3 km) from the upper reach; these profiles then display relatively constant, shallow slopes for most of the remainder of the profile (Fig. 4).

These bedrock channel profile groupings (Fig. 6) show both along-strike changes in profile character between domains and similarities in qualitative profile shape within each domain. In Figure 7, we plot the most important geomorphic indices used in our study (Table 1), including several measures discussed above, with footwall domains labeled and indicated by differences in shading.

Catchment area

Most channels that drain the Wassuk Range (flowing east from the range crest) display catchments with areas less than 20 km^2 along most of the range front, regardless of along-strike location (Figs. 4 and 7; Table 1). In the Shurz domain, channels display decreasing catchment area toward the south, from over 9 km^2 to less than 2 km^2, with the largest difference between the catchment areas for channels 5 and 6, where we subdivide the domain into North and South subdomains. These changes mirror the decrease in channel length and increase in average slope (Fig. 7; Table 1) discussed above.

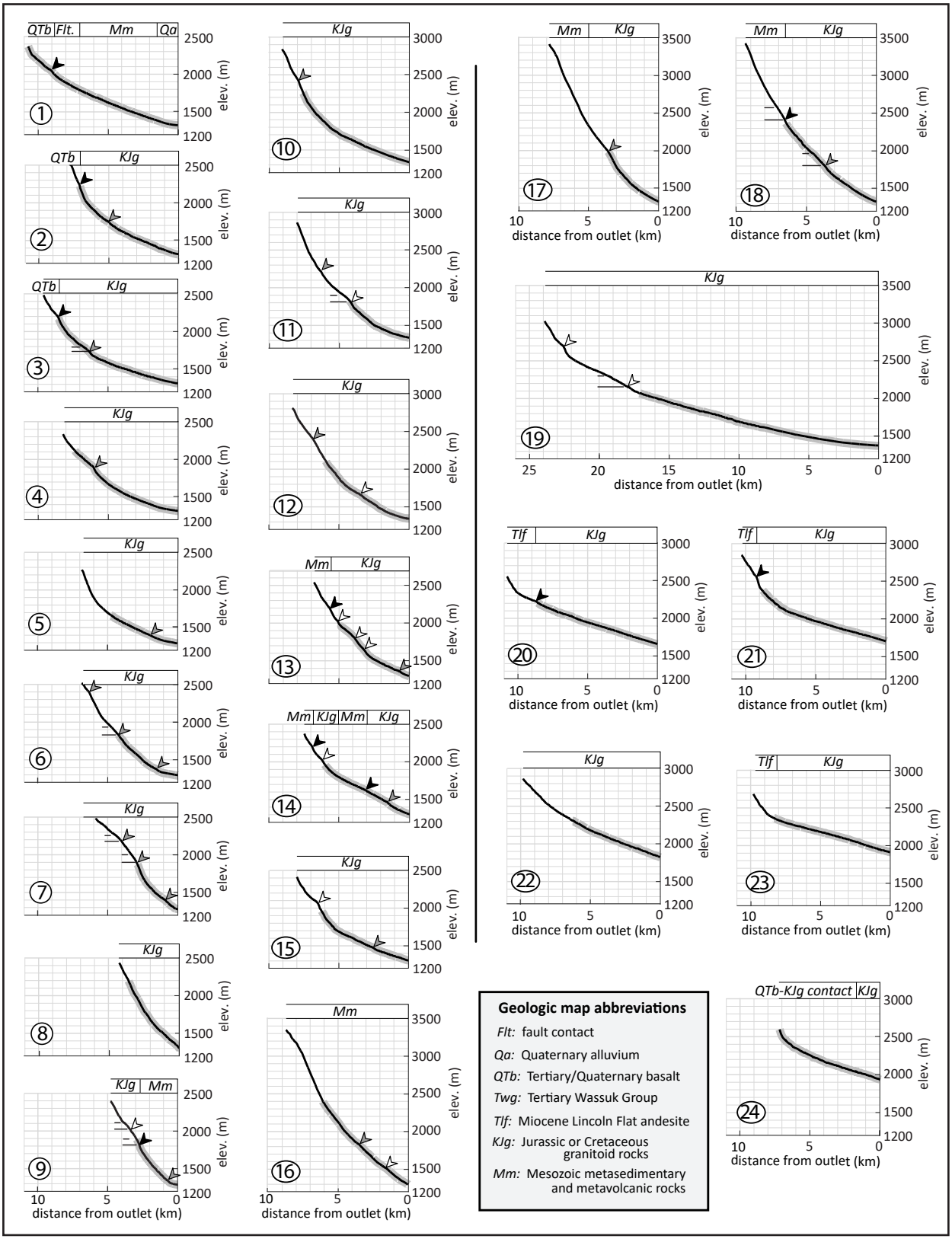

Figure 5. Long profiles of bedrock channels with knickpoints (arrows), convex reaches (elevation range delimited by horizontal lines), and geologic map units (abbreviated at top of each graph). The light gray highlighted section of each profile was used to derive ksn and concavity (θ) values listed in Table 1. Black knickpoint symbols mark hypothesized lithologic contacts, gray knickpoint symbols mark hypothesized fault locations, and white knickpoint symbols mark knickpoints with no known origin.

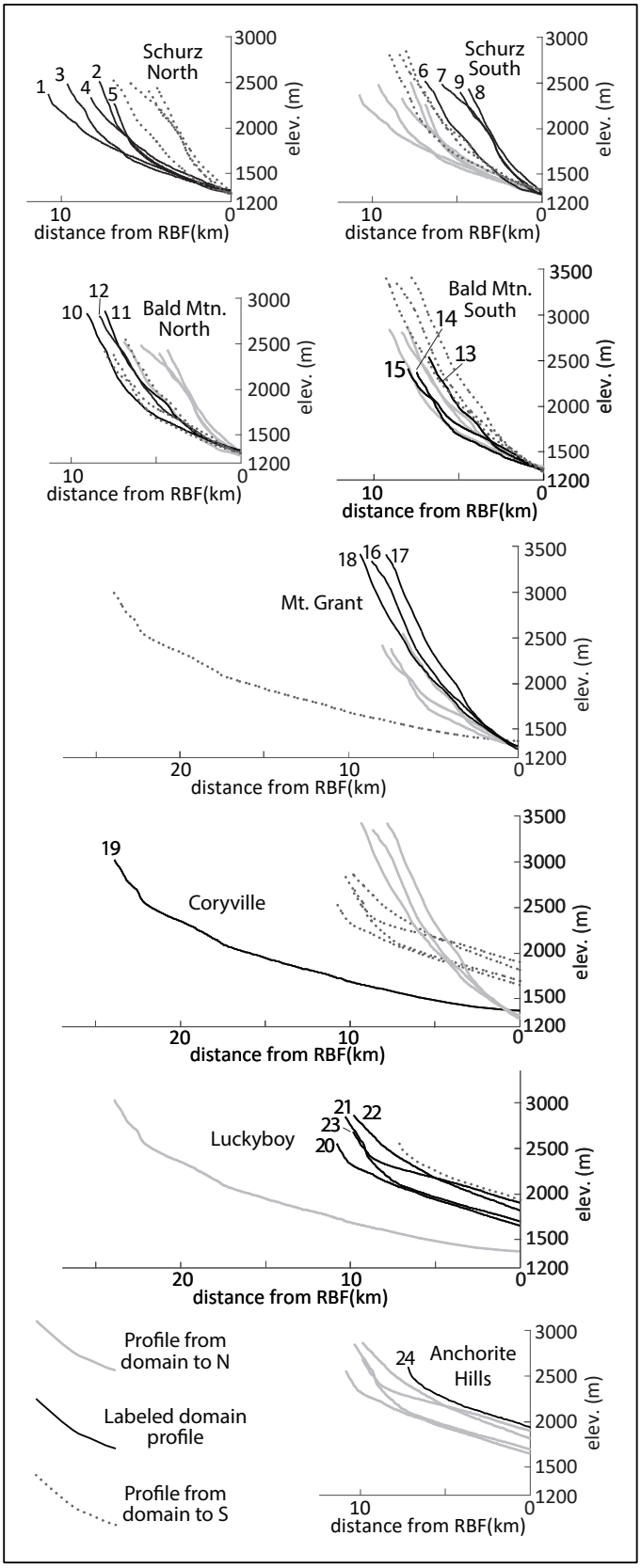

Figure 6. Bedrock channel profiles, shown from North (Shurz North) to South (Anchorite Hills). Black profiles are from the labeled domain, light gray profiles are from domain to north, and dashed profiles are from domain to south. See Figure 4 for map view traces of each channel.

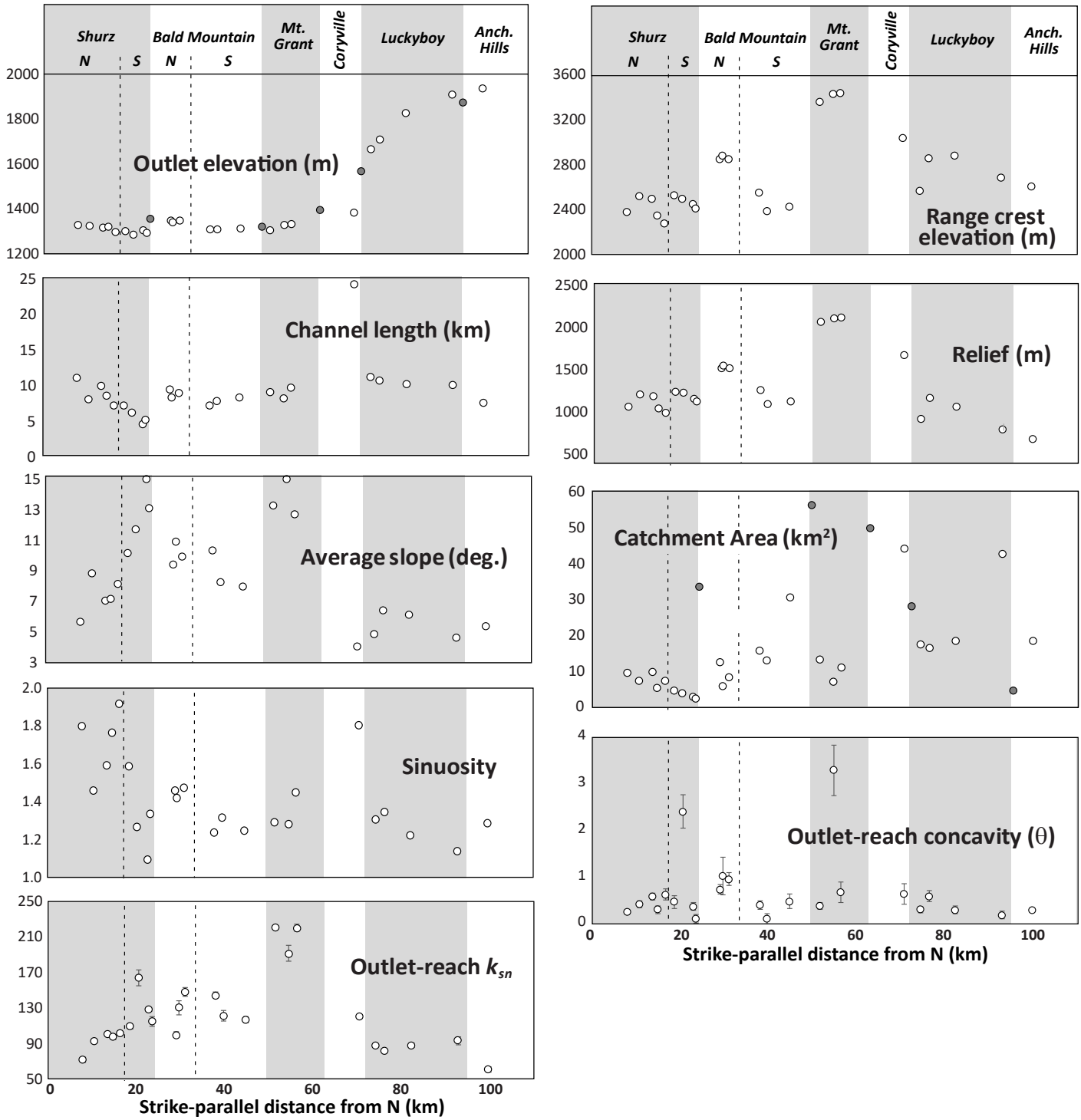

Figure 7. Bedrock channel data, plotted by strike-parallel outlet position along the Wassuk Range normal fault. Shaded regions indicate interpreted footwall domains, with North and South subdomains within the Shurz and Bald Mountain domains divided by vertical dashed lines. Domains and subdomains (N or S) are labeled at the top of each column. Data symbols shaded dark gray indicate watersheds (and associated outlets) with trunk streams that do not originate at a well-defined range crest (A-E in Fig. 4). For both outlet-reach ksn and outlet-reach concavity values, bars indicate two standard deviations (2σ). See Approaches and Methods for discussion of what constitutes a well-defined range crest.

Catchment areas from all domains to the south display average values higher than Shurz domain channels, with channels in the Coryville, Luckyboy, and Anchorite Hills domains displaying higher catchment areas than most channels in the Bald Mountain, and Mt. Grant domains (Figs. 4 and 7; Table 1). Within the Bald Mountain domain, channels 10-12, with outlets along the NNW-striking rangefront (North subdomain), display catchment area values smaller than channels 13-15, with outlets along the N- to NNE-striking rangefront (South subdomain) (Figs. 4 and 7; Table 1).

Interestingly, the catchment areas for channels that do not drain from a well-defined range crest (catchment areas A-E in Fig. 4; shaded gray dots in Fig. 7; Table 1) commonly contrast with catchment areas for adjacent channels to the north and south. In the case of A and B, these catchment area values are significantly higher than channels to the north and south (Figs. 4 and 7; Table 1). Catchment area C is also higher than those for channels north and south, but the contrast is not as significant, with the Coryville domain channel catchment area value similar to that for C (Figs. 4 and 7; Table 1). Catchment area D displays an area value transitional between channels in the Coryville and Luckyboy domains, and the catchment area E value is significantly lower than channels to the north and south (Figs. 4 and 7; Table 1).

Sinuosity

Bedrock channel sinuosity varies along the Wassuk Range, with values that in some cases can be related to average slope (Fig. 7; Table 1). For example, in the Shurz domain, channel sinuosity values generally decrease as average slope increases, especially evident in values from the South subdomain (Fig. 7; Table 1). However, channels in the Bald Mountain and Mt. Grant domains display relatively similar sinuosity values in spite of differences in average slope values for these channels (Fig. 7; Table 1). The Coryville domain channel displays a high sinuosity value that corresponds with a low average slope, but sinuosity values from the Luckyboy and Anchorite Hills domain channels cannot be similarly related to average slope, with sinuosity values that slightly increase or decrease along strike in concert with similar changes in slope (Fig. 7; Table 1).

Except for channels from the Shurz domain (general increase in slope and decrease in sinuosity along strike) and Coryville domain (low slope and high sinuosity values), we observe no clear correlation between sinuosity and average slope (Fig. 7), consistent with previous research investigating the same two variables for modeled (e.g., Schumm and Khan, 1972) and real-world (e.g., Miller, 1988; Prema et al., 2018) channelized systems. Our observations reveal that in the footwall of an active normal fault, bedrock channel sinuosity cannot be used to delineate along-strike changes in fault-related uplift rates. However, Prema et al. (2018) show that although there is no correlation between slope and sinuosity along a channel, the geological evolution of the terrain drained by a channel does impact that channel's sinuosity, with changes in sinuosity impacted by differences in tectonic forcing. Thus, abrupt changes in sinuosity in adjacent along-strike channels (e.g., Shurz S. vs. Bald Mountain N. channels; Bald Mountain N. vs. Bald Mountain S. channels) might indicate that adjacent channels drain footwalls of fault segments with different histories over long (~10^6-10^7 yr) time scales.

Channel steepness

Bedrock channels show relatively consistent normalized steepness values within each domain, with highest values near the fault trace (Fig. 4; Table 1). The highest k_{sn} values in the range occur in the Mt. Grant domain, with two channels displaying k_{sn} values of at least 175 for much of their length (Fig. 4). To both the north and south of Mt. Grant, values remain relatively constant between 75 and 150, with a decrease near the northern and southern terminations of the range (Fig. 4), consistent with the idea that the greatest steepness values along a normal fault should occur near the midpoint of the fault trace, with the lowest values near the termination of fault-related slip (e.g., e.g., Cowie and Scholz, 1992; Dawers et al., 1993; Dawers and Anders, 1995; Peacock, 2002). Importantly, all values along the Wassuk Range are consistent with k_{sn} indices expected for bedrock channels in tectonically active regions (e.g., Whipple, 2004).

To best characterize channel steepness associated with most recent motion along the Wassuk Range fault, we compare k_{sn} values from the reach closest to bedrock channel outlets along the eastern flank of the range (analyzed reaches shaded in Fig. 4). As with map-view k_{sn} values (Fig. 4), the outlet-reach steepness values for Mt. Grant domain channels, ranging from 190.5 (±9.0) to 220.4 (±3.6), are much higher than values from any other channels in the Wassuk Range (Fig. 7; Table 1). To the north and south of the Mt. Grant domain, channels from the Bald Mountain and Coryville domains display outlet-reach normalized steepness values between 100 and 150 (Fig. 7; Table 1). The contrast in k_{sn} values between the northernmost and southernmost Mt. Grant channels and the nearest along-strike channel in the Bald Mountain and Coryville domains, to the north and south, respectively, is extraordinarily large, at approximately 100 (channels 15 vs. 16 and 18 vs. 19) (Table 1; Fig. 7).

To the north, the range in k_{sn} values for Bald Mountain North and South subdomain channels are similar. The lowest k_{sn} value in each subdomain is located closest to the adjacent domain to the north (Shurz) and to the south (Mt. Grant) (Fig. 7; Table 1), and the highest normalized steepness value in each subdomain is adjacent to the boundary between North and South subdomains (Fig. 7; Table 1). Channels from the Shurz domain, with the exception of channel 7, display monotonously decreasing k_{sn} values from south to north (Fig. 7; Table 1), with values that decrease to a minimum of 72.1 (2σ ±3.0) for the northernmost channel of the Shurz North subdomain (Fig. 7; Table 1).

To the south of Mt. Grant, the Coryville domain channel displays a value of 120.6 (±2.1), and the Luckyboy domain channels display lower but relatively constant values between about 82 and 94, with low standard deviations (Table 1; Fig. 7). The Anchorite Hills domain channel displays the lowest k_{sn} value in the Wassuk Range, at 61.0 (±3.0) (Fig. 7; Table 1). Normalized channel steepness values change abruptly between all southern domains (Mt. Grant to Anchorite Hills) (Table 1; Fig. 7).

Channel concavity

Of the geomorphic measures analyzed in this study, outlet-reach concavity (θ) is least effective in delineating footwall domains. With the exception of two outlier outlet-reach concavity values (channels 7 and 17 from the Shurz and Mt. Grant domains, respectively), all domains but Bald Mountain North display similar values, with most channel concavity values within the 0.30 – 0.65 range (Table 1; Fig. 7). This range is similar to values expected (~0.4-0.6) in landscapes with well-equilibrated channels subjected to uniform rock uplift and active denudation (e.g., Kirby and Whipple, 2001; Tucker and Whipple, 2002; Wobus et al., 2006; Boulton et al., 2014), so the lack of significant changes between domains within the footwall of an active normal fault is not surprising. Although Bald Mountain North values are higher relative to most other channels (0.73 (±0.10) to 1.02 (±0.41)), these values, too, fall within the range of values outlined in the literature, within standard deviation. In the cases of outlier channels 7 and 17, the outlet reaches analyzed are downstream of knickpoints, with outlet reaches that differ, both qualitatively and quantitatively, from concavities of adjacent channels within each domain (Fig. 5).

Channel knickpoints and convexities

Faults or lithologic variations are responsible for many of the knickpoints and convexities identified on bedrock channel long profiles (Figs. 4 and 5). Minor (low-displacement) faults associated with the active range-bounding fault system on the east flank of the range likely cause aligned knickpoints from adjacent bedrock channels (Figs. 4 and 5). These include low-elevation knickpoints displayed on channels 5-7, 9, and 13-15 (Figs. 4 and 5). Alignments of knickpoints at higher elevations suggest faults within the footwall, which are usually difficult to detect in plutonic rocks (Figs. 2, 4, 5) without distinct strain markers. Because these knickpoints do not occur at the same elevations and do not display predictable changes in elevation along fault strike, we eliminate the possibility that these are migrating knickpoints that might indicate a transient response to a change in slip rate along the fault zone (e.g., Crosby and Whipple, 2006; Burbank and Anderson, 2012; Castillo et al., 2013; Boulton et al.,

2014). These alignments occur in channels 2-4, 6 and 7, 10-12, and 16-18 (Fig. 5). We do not attribute cause for the 8 remaining knickpoints shown on Figure 4 (white dots), but steep slopes present within these drainages commonly lead to slope instability, so some of these knickpoints may be caused by geologically recent, localized mass wasting events.

Statistical analysis of differences between domain populations

Although we cannot test the statistical significance of differences between the qualitative shapes of bedrock channel populations, especially as displayed in Figure 6, we do test the statistical differences between other geomorphic measures using T-test analysis, as described in **APPROACHES AND METHODS**. We focus on relief, channel length, straight-line distance, Z value, average slope, catchment area, sinuosity, and normalized steepness (Table 2). Our statistical analysis of the differences between adjacent bedrock channel populations confirms our proposed division of footwall domains and subdomains.

We consider our scaled relief-length value (Z), which takes into account both relief and channel length, to be the best indicator of morphologic differences between domain populations (Table 2). Our comparison of Z-values suggest that all adjacent along-strike domain and subdomain populations are statistically different at very high confidence (all adjacent populations >98% confidence). Likewise, statistical comparison of domain population relief and channel length values provides strong evidence of abrupt along-strike changes (Table 2).

Although abrupt increases or decreases in along-strike catchment areas can be used to aid identification of potential fault segment boundaries (Fig. 7; Table 1), the catchment areas of channel populations from adjacent domains do not consistently display statistical significant differences (Tables 2 and 3). Similarly, many differences between average slope and sinuosity values for populations of adjacent domains (or subdomains) are not significantly different along the Wassuk fault system (Table 2). However, the average slope, catchment area, and sinuosity values for the Coryville channel are all significantly different than domains to the north and south, and the Shurz North and South subdomain populations are significantly different for all three measures (Table 2).

Normalized steepness (k_{sn}) values from domains north of the Bald Mountain-Mt. Grant domain boundary do not display the abrupt changes in value that are displayed to the south of the boundary (Fig. 7; Table 1). T-test analysis supports this observation, with all adjacent along-strike domain channel populations significantly different (all confidence values >99%) south of the Bald Mountain South-Mt. Grant domain boundary (Table 2) and no statistically significant difference between adjacent domain populations from that boundary to the northern terminus of the Wassuk Range (Table 2). However, normalized outlet-proximal steepness values for the Shurz North and South subdomain channel populations are significantly different at high confidence (Table 2).

The impacts of lithology and climate on footwall morphology

In the Wassuk Range, lithology impacts long-channel profile characteristics but the effects of lithology are easily identified and do not significantly change our division of domain populations. Changes in lithology cause profile knickpoints (channels 2, 3, 9, 13, 14, 18, 20, 21) (Figs. 4 and 5), but we see no differences in geomorphic indices for domain populations that we can directly relate to lithology. For example, although bedrock channel 1 follows a fault trace for part of its upper reach (Figs. 2 and 4) and flows along a completely different lithology for most of its length (Mm) relative to other channels in the Shurz domain (KJg) (Fig. 5), most geomorphic indices are consistent with the channel's position within its domain (Table 1; Fig. 7). However differences in lithology may increase intra-population variability.

In the case of climate, previous workers have demonstrated that differences in precipitation rates may lead to significant discrepancies in normalized steepness values (k_{sn}), even when other tectonic variables are similar (e.g., Hijmans et al., 2005). This is true with latitudinal variations in climate affecting range relief (e.g., Champagnac et al., 2012), and differences in precipitation rates lead to

TABLE 2. CONFIDENCE VALUES BETWEEN POPULATIONS OF DOMAIN BEDROCK CHANNELS

	Domains compared	Shurz N - Shurz S	Shurz S - Bald Mtn. N	Bald Mtn. N - Bald Mtn. S	Bald Mtn. S - Mt. Grant	Mt. Grant - Coryville	Coryville - Luckyboy	Luckyboy - Anch. Hills
% confidence of diff. pop.	**Relief**	>90%	***>99.9%***	***>99.9%***	***>99.9%***	***>99.9%***	***>99.9%***	***>98%***
	Channel Length	***>99%***	***>99%***	***>95%***	>90%	***>99.9%***	***>99.9%***	***>99.9%***
	Straight-line distance	>90%	***>99.9%***	<50%	>80%	***>99.9%***	***>99.9%***	***>99.9%***
	Scaled relief-length value (Z)	***>98%***	***>99.9%***	***>99.8%***	***>99.9%***	***>99.9%***	***>99.9%***	***>99.9%***
	Average Slope	***>99.8%***	>90%	>80%	***>99%***	***>99%***	***>95%***	<50%
	Catchment area	***>99.8%***	***>95%***	>90%	>80%	***>99.9%***	***>95%***	>50%
	Sinuosity	***>98%***	>70%	***>99.8%***	>70%	***>99%***	***>99.9%***	>50%
	Outlet Reach k_{sn} value	***>98%***	>70%	<50%	***>99.8%***	***>99%***	***>99.9%***	***>99.8%***

The confidence values listed above are based on the t-test values displayed in Table S1. Confidence values that are 95% or higher (bold-faced, italic) suggest statistically significant differences between sample populations.

changes in channel slope (e.g, Bookhagen and Strecker, 2012; D'Arcy and Whittaker, 2014). Because the Wassuk Range trends approximately NNE for much of its length (>100 km), latitudinal changes in precipitation could impact channel slope, range relief, and other geomorphic indices.

Modern precipitation data from the Wassuk Range (Lopes and Medina, 2007) (Table 3) suggest that precipitation in adjacent domains vary by range-crest elevation and not by latitude. Assuming that a similar magnitude of elevation-based precipitation variation is consistent across a range of timescales ($10^1 – 10^7$ yrs), this elevation-precipitation rate correlation requires that domains with higher elevations should have experienced greater erosional denudation relative to lower elevation domains (assuming similar lithologies), consistent with the findings of D'Arcy and Whittaker (2014), who found a positive coupling between uplift rate and precipitation rate in the production of elevation in tectonically active areas. However, our goal is to analyze geomorphic differences between adjacent domains in order delineate fault segments along the Wassuk range front. Therefore, although *quantification* of differences in uplift rate between adjacent domains would be difficult to extract from geomorphic data because of the complicating role of precipitation-related erosion in producing elevation (e.g., D'Arcy and Whittaker, 2014), we are confident that the differences in geomorphic indices described above permit us to relate the normal fault footwall morphology to along-strike fault segments and segment boundaries.

FOOTWALL DOMAINS AND FAULT SEGMENTATION

Discontinuities in the Wassuk range crest, differences and similarities of geomorphic indices between and within along-strike domains, and abrupt changes in catchment areas of outlet channels relate directly to the long-term (10^6-10^7 yr) behavior of fault segments and segment boundaries. We hypothesize that mechanical coupling between segments varies along strike, with some adjacent segments hard linked and others with weaker coupling. We propose a segment structure for the Wassuk Range (Fig. 8), including both primary and secondary segments (e.g., Manighetti et al., 2015), and we summarize geomorphic data for each domain and subdomain in Table 3. Importantly, abrupt strike-parallel changes along the Wassuk fault require structures, in the form of either faults or folds, at high-angles to the Wassuk fault to accommodate differential uplift and tilt between footwall blocks (e.g., Faulds and Varga, 1998).

Fault segments and accommodation structures

The Schurz domain displays a well-defined and continuous NNW-trending range crest (Fig. 4) with footwall relief and Z value that increase to the SSE (Table 1; Fig. 7) coincident with an increase in average channel slope (Fig. 7). The range crest within the Schurz domain loses definition approximately 18 km SSE of its northernmost extent, and to the south, the range crest becomes well-defined again approximately 5 km to the south and west, in the Bald Mountain domain. In addition, the catchment area of the channel that drains the region between domains displays a value nearly three times the values of the southernmost Shurz channel and the northernmost Bald Mountain channel (Table 1; Fig. 8). This discontinuity and the large right step in the map-view trace of the range crest (Fig. 4), the sudden increase in catchment area, and the change in channel profile properties coincide with the Penrod Canyon fault complex (PCF in Figs. 2 and 8), a Miocene-age accommodation zone (Dilles, 1993).

Geomorphic indices from the Mt. Grant domain display evidence for the highest uplift rate along the Wassuk fault, with a decrease in footwall uplift and hanging wall subsidence to the north and south, consistent with displacements that decrease to zero at the tips of normal fault systems (e.g., Cowie and Scholz, 1992; Dawers et al., 1993; Dawers and Anders, 1995; Peacock, 2002) However, breaks in range-crest continuity, large increases in outlet channel catchment area, and abrupt changes in domain channel characteristics north and south of Mt. Grant suggest that mapped cross-range faults (e.g., John, 1983; Gorynski et al., 2013) must accommodate differences in rates of footwall uplift (Figs. 2, 4, 7, and 8). A scoop-shaped, east-dipping normal fault bounds the west and north sides of the Mt. Grant

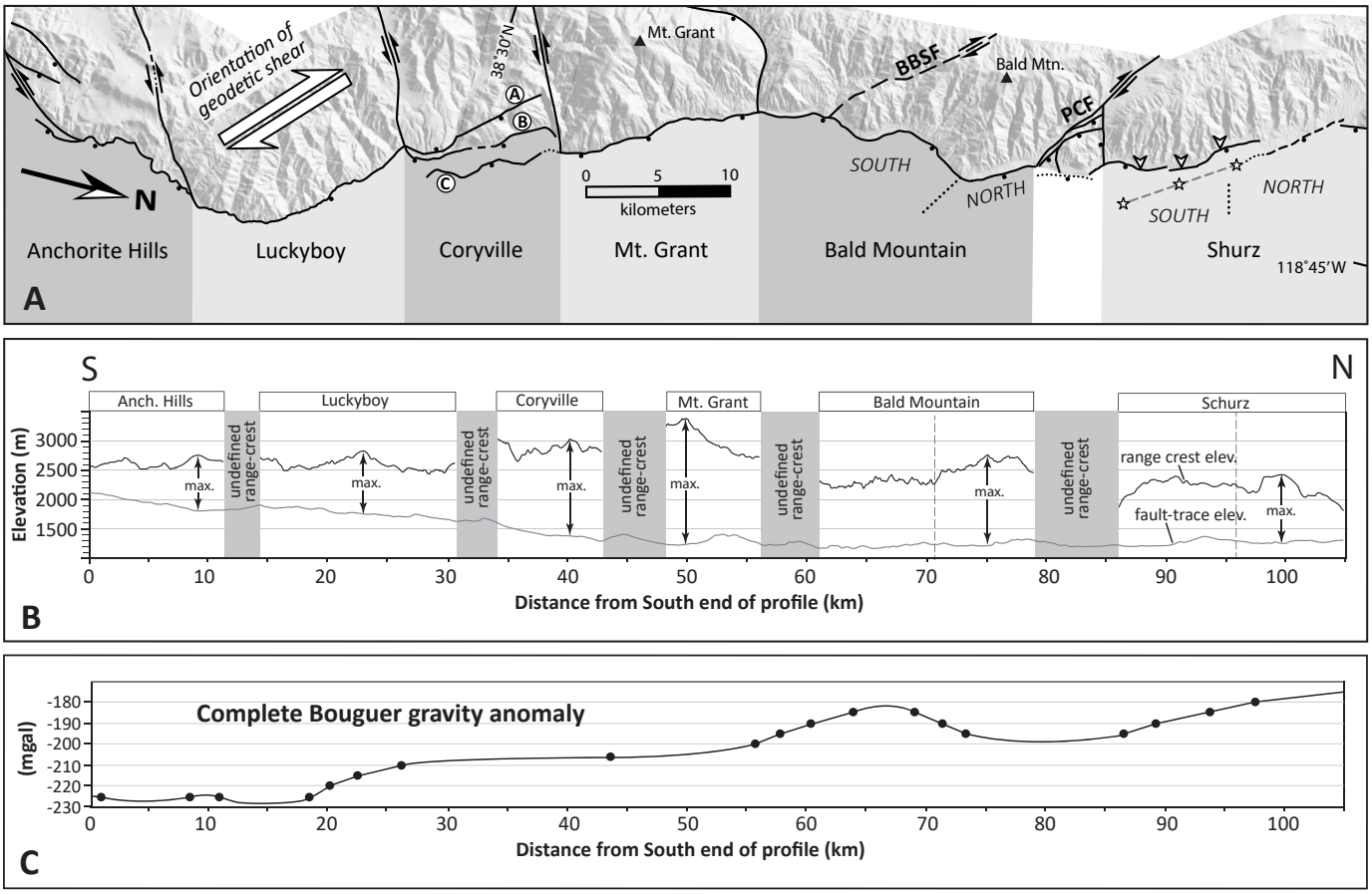

Figure 8. A. Proposed primary (shaded) and secondary ("NORTH" AND "SOUTH") fault segments of the east-dipping Wassuk Range normal fault. Mapped faults A-C accommodate extension along the range front of the Coryville footwall domain. Large white arrows indicate orientation of modern dextral shear indicated by geodetic data (orientation from Hammond et al., 2009; Bormann et al., 2016). Note proposed SSE-ward projection (starred, gray fault) of mapped fault segment that bounds the North sub-segment of the Shurz domain. The authors propose that the present-day fault segments that bound the east flank of the range (marked with white triangles) now accommodate strain originally taken up by the "starred" fault. See text for discussion. B. Strike-parallel range-crest and fault-trace elevation profiles from the Wassuk Range. Gray shaded boxes indicate locations where the range crest is not topographically well-defined. The difference between the range-crest and fault-trace profiles is footwall relief, which is highest near the central Wassuk Range and decreases to the north and south. Arrows indicate location of maximum footwall relief, regardless of channel position, within each fault domain. C. Complete Bougeur gravity anomaly profile from the Walker Lake basin, east of the Wassuk Range fault. Circles are data points from a line approximately 3 km east of the Wassuk fault and are based on the complete Bouguer gravity anomaly map of Saltus (1988).

TABLE 3. SUMMARY OF KEY DATA FROM WASSUK RANGE FOOTWALL DOMAINS

Block		Footwall relief ave. (±σ) (m)	Straight line dist. ave. (±σ) (km)	Scaled length-relief ave. (±σ) (Z)	Catchment area ave. (±σ) (km^2)	Outlet-reach k_{sn} ave. (±s)	Ave. Rangecrest Precip. (cm/yr)**
Schurz	**North**	1080 (±95)	5.13 (±1.02)	7.95 (±1.97)	7.44 (±1.79)	93.0 (±12.3)	23-28
	South	1167 (±55)	4.13 (±0.46)	5.05 (±1.13)	2.94 (±0.99)	129.1 (±24.4)	23-28
Bald Mountain	**North**	1506 (±19)	5.92 (±0.31)	9.38 (±0.49)	8.41 (±3.41)	126.7 (±23.8)	28-33
	South	1137 (±87)	5.89 (±0.50)	6.73 (±0.44)	19.34 (±9.48)	127.8 (±15.0)	25-28
Mt. Grant		2007 (±26)	6.48 (±0.34)	12.16 (±0.64)	9.95 (±3.05)	210.3 (±17.1)	33-41
Coryville*		1651	13.31	28.98	43.78	120.6	33-36
Luckyboy		962 (±163)	8.17 (±0.39)	9.63 (±0.73)	23.33 (±12.72)	88.0 (±4.9)	28-33
Anchorite Hills*		661	5.59	5.11	18.12	61.0	25-30

*One channel analyzed

**1971-2000 Annual Average (Lopes and Medina, 2007)

domain; the location of this fault coincides with the highest channel catchment area in the Wassuk Range (channel B; Table 1; Figs. 2, 4, 7, and 8), much higher than the catchment area for domain channels to the north (Bald Mountain domain) and south (Mt. Grant domain). A scissor-sinistral-slip fault bounds the south side of the Mt. Grant domain and coincides with channel C, which displays the second-highest catchment area along the Wassuk Range (Table 1; Figs. 2, 4, 7, and 8). The Mt. Grant range crest is isolated from range crests to the north (Bald Mountain domain) and south (Coryville domain), with large step-overs relative to range crests to the north (left step-over) and south (right step-over) (Fig. 4).

Further south, abrupt changes in geomorphic indices and range-crest discontinuities coincide with the locations of other accommodation structures (Figs. 2, 4, and 8). Although there is no stepover in the map-view trend of the range crest between the Coryville and Luckyboy domains, the range crest loses definition between them (Fig. 4). The location of channel D, which drains from this poorly-defined range crest, coincides with a mapped scissor-sinistral-slip fault mapped by Gorynski et al. (2013) (Figs. 2, 4, and 8). The map-view relationship between the Luckyboy and the Anchorite Hills domains suggests that the change in dominant range-front fault strike, from NW to NE, might play a role in the differences between footwall morphologies, and the mapped NE-striking-scissor sinistral fault (Gorynski et al., 2013) provides a structure to accommodate differences in slip and block rotation between those domains (Fig. 8).

We suggest that the loss of range-crest continuity and, in several cases, the abrupt changes in channel catchment areas, are related to a combination of: 1) fault damage zones proximal to cross-range faults that promote localized high erosion rates and denudation; and 2) lower rates of slip and related footwall uplift approaching segment boundaries, which is predicted along segmented normal fault zones (Fig. 3). Importantly, with the exception of the BBSF, which is not well defined as it cuts across the Wassuk Range and does not separate Bald Mountain subdomains (Fig. 2), we consider the intersections between cross-range faults and the east-dipping Wassuk fault to be the approximate locations of boundaries between fault segments that have accommodated different total displacements and average slip rates over time.

Fault segment boundary geometries and earthquake rupture propagation

The length of our proposed 6 primary fault segments range from approximately 10 km for the Coryville segment to more than 15 km for both the Bald Mountain and Shurz segments (Fig. 8). These proposed lengths and the number of segments along the Wassuk Range are consistent with many active normal faults worldwide (e.g., Manighetti et al., 2009; 2015 *and references therein*). From the Luckyboy segment to the northern termination of the Wassuk Range, NNW-striking segments display a right-stepping, en echelon geometry, with 1-3 km offsets between most segments, while the Anchorite Hills and southern Luckyboy segments strike NE (Fig. 8). We use Wong et al.'s (2016) normal fault segment interaction models (Fig. 3) to propose how each segment boundary and mapped fault geometry would affect the lateral propagation of rupture and associated slip during earthquakes.

Anchorite Hills - Luckyboy segment boundary

The Anchorite and Luckyboy segments adjacent to the boundary display a relatively continuous NE-striking fault trace along the range front, with a small (~1 km) right step at the segment boundary (Figs. 2 and 8), coincident with the scissor-sinistral-slip fault mapped by Gorynski et al. (2013). This is the only boundary along the Wassuk normal fault with adjacent NE-striking segments (Fig. 8). Although geomorphic indices of the footwall suggest greater slip along the Luckyboy segment (Fig. 7; Table 3), the changes in slope along bedrock channels associated with the two segments are remarkably similar to each other and different from all channels associated with segments to the north (Figs. 5 and 6).

Results indicate that the Anchorite Hills segment is the least active segment of the Wassuk normal fault, so would be unlikely to independently generate large earthquakes. Thus, the boundary would more likely interact with southward-propagating ruptures. The presence of the scissor-sinistral

fault at the boundary might absorb some energy, but the relatively minor right step in the fault would be unlikely to be a significant barrier to rupture during a major (several-meter displacement) normal fault-generated earthquake (e.g., Wesnousky, 2006; 2008). Based on these observations, we propose a master-subsegment relationship (Fig. 3C), with rupture along the Anchorite Hills segment dependent on southward propagation of rupture from the Luckyboy segment. Rupture propagation during a small to moderate earthquake north of the segment would likely stop at the boundary, or at least display only minor overlap (Fig. 3B), while in a major earthquake, rupture would propagate through the segment boundary, with a decrease in slip adjacent to the boundary.

Luckyboy-Coryville segment boundary

The Coryville segment, best defined by fault segment "B" along the rangefront (Fig. 8A), also displays two previously-mapped (Gorynski et al., 2013) fault segments, with fault "A" likely connected to the Luckyboy segment to the south and fault "C" connected to the Mt. Grant segment to the north (Fig. 8A). The boundary between Luckyboy and Coryville segments displays a small (1-2 km) right step that also coincides with the intersection of the scissor-sinistral fault with the rangefront fault system. As stated above, the right step between segments is not of sufficient magnitude to be a barrier to rupture during a major earthquake (e.g., Wesnousky, 2006; 2008), but it likely does result in energy lost at the segment boundary. Based on the fault geometry at the Luckyboy-Coryville segment boundary, lateral earthquake rupture propagation along the rangefront would display different strengths of mechanical linkage that depend on propagation direction.

A northward-propagating rupture from the Luckyboy segment would lose significant energy due to slip propagating along segment "A," which is optimally-oriented (subparallel strike) to take up significant energy and slip associated with rupture propagation. A rupture propagating from the north along the Coryville segment ("B" in Fig. 8A) would likely propagate across the boundary more easily than from the south, with less energy lost as some fraction of total slip. In moderate earthquakes, a north-propagating rupture would likely display characteristics of overlap/triggered slip (Fig. 3B), with slip propagating past the boundary but at lower displacements, setting up an altered stress field that might trigger later slip on the Coryville segment. In contrast, we would expect characteristics of a multi-segment system (Fig. 3D) for a south-propagating rupture, with a reduction in slip adjacent to the boundary without significant rupture impedance.

We also suggest that in major earthquakes, the fault-parallel slip profile would display features of a hard-linked, multi-segment system (Fig. 3D) with rupture that propagates across the segment boundary, with perhaps a greater reduction in total slip at the boundary for a northward propagating rupture. Importantly, and with the possible exception of a triggered, small- to moderate-magnitude event (described above), we consider the Coryville segment too short (e.g., Wong et al., 2016) to independently generate major earthquakes.

Coryville-Mt. Grant segment boundary

The Coryville-Mt.Grant segment boundary displays a right step (~2 km offset) between segments that coincides with the intersection of the cross-range scissor-sinistral fault (Fig. 8A). Both segments are relatively linear in map view, but, similar to the Luckyboy-Coryville boundary to the south, fault geometry at the segment boundary suggests different rupture behaviors depending on propagation direction. A rupture propagating toward the south from the Mt. Grant segment would lose significant energy to the propagation of slip along segment "C," which dies out to the south, outboard (east) of the Coryville segment (Fig. 8A). In contrast, a rupture propagating toward the north from the Coryville segment would likely display a decrease in slip adjacent the boundary, but the right step at the boundary is not sufficient to be a significant barrier to the propagation of slip during a major earthquake (e.g., Wesnousky, 2006; 2008). Based on these observations, the boundary would likely behave as a multi-segment boundary for northward-propagating rupture (Fig. 3D) and as an overlap/triggered slip boundary for southward-propagating rupture (Fig. 3B).

Mt. Grant-Bald Mountain segment boundary

In map view, the Mt. Grant-Bald Mountain segment boundary displays a relatively continuous trace along the range front, without any significant en echelon step. However, the boundary location coincides with the map-view trace of the scoop-shaped normal fault mapped by Gorynski et al. (2013) (Figs. 2 and 8A), suggesting that slip propagating from either direction would lose energy at the fault intersection, resulting in a reduction in slip adjacent to the boundary. This geometry indicates similar multi-segment behavior (Fig. 3D) for slip propagating from north or south, with some impedance at the boundary.

Bald Mountain-Shurz segment boundary

The geometric relationship between the Bald Mountain and Shurz segments suggests the boundary would significantly impede or even arrest rupture propagation during an earthquake. The segment boundary coincides with two ~1 km en echelon steps in the range bounding system, right- and left-stepping, on either end of a short (<5 km) segment outboard (east) of both the Bald Mountain and Shurz segments (Figs. 2 and 8A). This short segment is adjacent to the cross-range Penrod Canyon fault complex (PCF in Fig. 8A), a zone highly deformed by earlier normal faults and a strike-slip fault that cuts across the Wassuk Range (Figs. 2 and 8A). The Bald Mountain segment terminates at the PCF, which displays a strike similar to the Bald Mountain segment.

This geometry, with the PCF more favorably oriented than the Shurz segment to the north, suggests that a northward-propagating earthquake would lose significant energy at the northern segment boundary, with the highly-faulted PCF (Fig. 8A) absorbing a portion of that energy and perhaps even arresting rupture, consistent with field-based scarp analysis of past ruptures by Demsey (1987). Because analysis presented in this paper suggests that the Shurz displays displacement-related uplift that rapidly decreases to the north, with topographic expression of the range ending just north of bedrock channel 1, the Shurz segment would be unlikely to independently generate significant earthquakes. Thus, we would expect the Bald Mountain-Shurz segment boundary to exhibit behaviors consistent with a master-subsegment relationship (Fig. 3C), with slip propagating north of the boundary only in large magnitude events.

Secondary segment boundaries

Within the primary Bald Mountain segment, the secondary North segment, east of Bald Mountain, strikes to the NNW and has a different footwall morphology and smaller channel catchment areas relative to the South secondary segment (Table 3), which displays a more sinuous map-view trace (Fig. 8A). Although mapped as a continuous fault along the entire South segment, fault orientation changes along strike, with right steps between NNW-striking segments. Right steps are located where the Buck Brush Springs fault (BBSF) intersects the range-bounding fault and between the outlets of bedrock channels 13 and 14 (Figs. 4 and 8). Although there are fundamental differences between the footwall morphology of North and South secondary segments, controlled by differences in fault related uplift along strike, the boundary between the segments cannot be well-defined along the range front. Thus, boundary geometry would not impact earthquake slip propagation, with differences in along-strike dip-slip displacement (North vs. South) potentially affected by different fault zone properties and/or the difference in fault orientation. Therefore, we do not classify the secondary-segment boundary using the model of Wong et al. (2016) (Fig. 3). However, a northward-propagating rupture might lose some energy along the BBSF, which is subparallel to the NNW-strike of the southernmost section of the Bald Mountain South segment (Figs. 2 and 8A).

The secondary segments of the Shurz segment are more intriguing; although geomorphic properties appear to change at a relatively constant rate along strike (e.g., Figs. 4 - 7), a significant change occurs between bedrock channels 5 and 6 (Tables 1-3; Figs. 4 and 5), which coincides with a 1-2 km right step between mapped secondary segments (Figs. 2 and 8). Although not a large enough right step to arrest rupture propagation during a major earthquake (e.g., Wesnousky, 2006; 2008), we

hypothesize that even in a major earthquake with a source far to the south, by the time slip propagates along the Shurz segment (white triangles in Fig. 8A), slip-related energy may not be sufficient to propagate through the secondary segment boundary. Thus, the boundary would likely behave as either a multi-segment boundary or as an overlap/triggered slip boundary, depending on the magnitude and location of the earthquake.

In order to explain the relatively significant change in footwall morphology from north to south, we suggest that the Shurz segment may once have been continuous along strike of the northern segment, with a projected position similar to the starred fault trace displayed in Figure 8A. Because pre-4 Ma dextral strike-slip displacement took place along the PCF (McIntyre, 1990; Dilles, 1993), when significant rates of extension began at ~4 Ma, the location of the range-front segments may have been controlled by that earlier dextral offset. If correct, the projection of the North segment would result in a right step of ~5 km relative to the Bald Mountain segment, and if northward propagating earthquake rupture dominated the segment boundary (as we propose here), we would expect NNW-directed propagation of a fault tip from near the present-day Bald Mountain-Shurz segment boundary to its present position bounding the southern flank of the range (segment marked by white arrows in Fig. 8A), resulting in a shorter right step and more efficient geometry for rupture propagation. This would necessarily shorten the distance between the range crest and the active fault, resulting in fundamentally different channel properties from south to north and causing the fault segment projected from the north segment (starred in Fig. 8A) to become inactive over a large number of earthquake cycles.

Summary

Our geomorphic analysis, when combined with mapped fault geometries and proposed segment boundary mechanical interactions, supports a model where the Mt. Grant segment has the highest probability of being the rupture source for a normal-fault generated earthquake, with probabilities that decrease with distances north and south of that segment. We also propose that the Wassuk Range fault system has matured to the point that no fault segment behaves completely independently (Fig. 3A), with segments potentially branching from a deeper master fault system, similar to the architecture suggested by the 1915 Pleasant Valley earthquake rupture pattern (e.g., Wallace, 1984; dePolo et al., 1991; Ferrill et al., 1999). The Mt. Grant and Bald Mountain segments should rupture (~35 km total) during any major ($>M_s$ 7) earthquake that nucleates along either segment, with greater rupture length possible, dependent on location and magnitude, consistent with Demsey's (1987) analysis of fault scarps along the Wassuk Range. The relatively long (~18 km) Luckyboy segment may also be capable of generating a major earthquake, with rupture that would likely propagate southward into the Anchorite Hills segment and northward through the Coryville segment and into at least the Mt. Grant segment.

The geometries of segment boundaries on both ends of Coryville segment should impede or even arrest earthquake rupture from the north or the south, a hypothesis supported by the fundamentally different footwall morphologies in the Luckyboy and Anchorite Hills blocks (Fig. 6) relative to all blocks to the north. In addition, the presence of the PCF at the Bald Mountain-Shurz segment boundary (Figs. 2 and 8) presents a geometry that would likely arrest northward propagation of slip, as suggested by the lack of young fault scarps north of PCF (Demsey, 1987). The Anchorite Hills and Shurz segments should not be capable of generating large earthquakes, with most of these segments' long-term cumulative displacement attributed to slip propagating from earthquakes north or south, respectively, making them dependent on adjacent segments. The Coryville, Anchorite Hills, and Shurz segments should not be capable of being rupture sources for major earthquakes.

The Wassuk fault zone and basin gravity data

Although displacement fields from the footwall and the hanging wall of a normal fault are rarely symmetrical or equal in magnitude to each other (e.g., Savage and Hastie, 1966; Masiha and Smylie, 1971; Gibson et al., 1989), Wu and Bruhn (1994) used geologic data from the footwall and gravity data from the hanging-wall basin of the South Oquirrh Mountains fault zone (Utah) to demonstrate that

cumulative fault displacement patterns indicated by geologic data correspond to patterns in measured gravity signatures. We document a similar pattern for the Wassuk Range fault zone, where gravity data support our proposed segmentation from the Mt. Grant segment to the northern termination of the range and may imply a fundamental change in sedimentation and/or fault dynamics south of the Coryville segment.

Bouguer gravity anomaly values (Saltus, 1988) from the hanging wall basin (approximately 3 km east of the fault), from the northernmost extent of the range to the Mt. Grant segment, reveal that the lowest gravity values, associated with the greatest thicknesses of sediments in the hanging wall (e.g., Blakely, 1995), occur adjacent to the highest range-crest elevations (Fig. 8). Gravity values decrease from (-) 180 mgals to below (-) 200 mgals from the northernmost extent of the defined Wassuk range crest to the southernmost extent of the Shurz segment range crest (Fig. 8C). Gravity values remain low adjacent to the PCF and the Bald Mountain North secondary segment but increase above (-) 195 mgal adjacent to the Bald Mountain South secondary segment, which displays lower range relief adjacent to either the Bald Mountain North secondary segment or the Mt. Grant segment to the south (Figs. 8B and 8C).

However, this relief-gravity relationship is not well-defined south of the Mt. Grant segment, where basin gravity values decrease rapidly from approximately (-) 210 mgals to below (-) 225 mgals nearly coincident with the change in strike along the Luckyboy segment (from NNW- to NE-striking) (Fig. 8). Interestingly, from the northernmost tip of the Luckyboy segment to the southernmost extent of the Wassuk Range to the southwest, outlet elevations increase to values far above any other outlet elevations along the fault system (Figs. 7 and 8). We propose that some combination of a change in sedimentation pattern and the shift from normal dominated to oblique normal-sinistral kinematics might cause the change in gravity values parallel to the fault zone. Because the elevation of the range crest does not change significantly in spite of decreasing relief (Fig. 8B), it is possible that a thicker package of sediments is present outboard of the rangefront resulting in lower gravity values. This is consistent with basin formation in a transtensional environment associated with the Mina Deflection to the south (e.g., Oldow et al., 2001; 2008), which is approximately bound by the Anchorite Hills segment of the Wassuk fault on the north (Fig. 1).

IMPLICATIONS

An improved geomorphic analysis protocol

Although recent studies worldwide have investigated strike-parallel variation in footwall morphology using well-developed geomorphic tools (e.g. Papanikolaou et al., 2013; Rossi et al., 2017; He et al., 2018), previous researchers did not explicitly define or analyze the mechanically-significant segments and segment boundaries that could impact earthquake rupture along those fault zones. In this study, we integrate strike-parallel loss of range-crest continuity, abrupt changes in channel catchment areas, and differences in footwall geomorphic character to identify persistent segment boundaries that are crucial to understand earthquake rupture dynamics (e.g., Wong et al., 2016). We have combined our results with previous investigations of the Wassuk fault (Demsey, 1987; McIntyre, 1990; Dilles, 1993; Stockli et al., 2002; Krugh, 2008; Surpless, 2010; 2011; Gorynski et al., 2013; Surpless and Kroeger, 2014) to provide a detailed analysis of how propagating earthquake ruptures might interact with the geometries of segment boundaries.

Had this been a poorly-studied fault zone, results from our analysis protocol would permit a targeted investigation of both the segmented fault system and the normal fault footwall. In addition to identifying the locations of fault segment boundaries and potential cross-range accommodation structures (e.g., the cross-range faults that dissect the Wassuk fault footwall), investigators could evaluate the potential roles of lithology and unmapped faults within the footwall. These results would

also guide geologic mapping and sampling for geochronologic, thermochronologic, or cosmogenic nuclide studies of uplift, structural tilting, and erosion, providing quantitative data to integrate with initial analysis. Further, because of the paucity of paleoseismic research along the Wassuk normal fault, our results can be used by future researchers to design studies that target key segment boundaries for investigation, eventually revealing greater detail about how each of these boundaries controls normal fault rupture during major earthquakes.

Major earthquakes on segmented normal faults

Our fault segmentation and segment boundary model for the Wassuk Range is consistent with previous studies of historical worldwide surface faulting, with lateral rupture lengths for normal and oblique-normal events most commonly 15 to 40 km (Wells and Coppersmith, 1994; Wells, 2013) and the longest historical surface rupture 95-101 km long for the 1887 earthquake in Sonora, Mexico (Suter, 2008; 2015; Wong et al., 2016). Previous workers have demonstrated the importance of fault segmentation in controlling normal fault earthquake surface rupture for a number of faults in the western U.S., including the 1915 Pleasant Valley, Nevada, earthquake (Wallace, 1984), the 1983 Borah Peak, Idaho, earthquake (Crone et al., 1987), late Quaternary ruptures along the range fronts of the Lemhi, Beaverhead, and Tendoy ranges (Crone and Haller, 1991), and interpreted rupture segments for past earthquakes along the Wasatch fault zone in Utah (Wong et al., 2016).

These studies support our interpretation of segment boundaries along the Wassuk Range, with rupture along the entire fault zone unlikely due to geometric barriers to propagation (e.g., PCF or Coryville fault geometries). We also posit that the segmentation and segment boundaries presented here support previous investigations of faults worldwide, which display similar amounts of relative displacement at the same along-strike segments on a given fault (e.g., Klinger et al., 2011; Hecker et al., 2013 *and references therein*; Wong et al., 2016). Our results also imply a relative consistency of lateral rupture extent and similarity of segment boundary behavior over many earthquake cycles (e.g., Aki, 1979; 1984; Elliott et al., 2015; Wong et al., 2016).

The central Walker Lane geologic-geodetic data discrepancy

We have treated the Wassuk Range fault system normal fault dominated by dip-slip displacement over time, consistent with geologic studies across the Walker Lane at this latitude (e.g., Ramelli et al., 1999; Surpless et al., 2002; Schweickert et al., 2004; Kent et al., 2005; Surpless, 2008; Cashman et al., 2009; Surpless and Kroeger, 2014). However, recent geodetic data and related block modeling studies across the region (e.g., Hammond et al., 2011; Bormann et al., 2016) reveal a modern strain field consistent with nearly pure dextral shear (~8 mm/yr) across this same region, trending approximately N45°W, with no significant E-W-oriented extensional strain component (see Fig. 8A for geodetically-defined shear). Although the preferred Bormann et al. (2016) block model, constrained by geodetic data and mapped normal faults, requires ~2 mm/yr dextral slip be accommodated by the Wassuk Range fault zone (Fig. 1), the model permits normal slip along the Wassuk fault zone, consistent with paleoseismic studies and fault scarp analysis of Holocene displacements (e.g., Demsey, 1987; Bormann et al., 2012; Surpless and Kroeger, 2014).

The Wassuk fault zone is predominantly a right-stepping, NNW-striking, en echelon fault with NNE- or NE-striking stepovers (Figs. 2 and 8), which suggests that accommodation of geodetically-determined NW-oriented dextral shear should result in different types of slip that depend on fault plane orientation. Although the northern section of the Luckyboy segment and the Shurz segment are subparallel to dextral shear indicated by geodetic data (<10° difference) (Fig. 8A), the mapped traces of the Coryville, Mt. Grant, and NNW-striking sections of the Bald Mountain segment are at angles of 10-15° to modern shear strain (Fig. 8A). This would suggest dextral slip with a small (<0.3 mm/yr) dip-slip component along the Coryville, Mt. Grant, and portions of the Bald Mountain segments, and nearly pure dextral slip along the Luckyboy and Shurz segments. In contrast, the significant right steps within the

Bald Mountain segment strike approximately N40°E, nearly perpendicular to the indicated shear, suggesting nearly pure normal dip-slip displacement along those short sections of the fault. Near the southern terminus of the range, the Anchorite Hills segment also displays a NE strike (Fig. 8A), indicating nearly pure dip-slip normal displacement would be expected along that segment in the modern strain field. However, because the Anchorite Hills segment is on the northern margin of the complexly deforming Mina Deflection (Fig. 1), so we have less confidence in predicting slip behavior along that segment.

Although we can predict the expected modes of slip during future earthquakes along the segmented Wassuk fault zone based on recent geodetic data, we find no evidence of a fundamental change in strain accommodation along the fault zone. The topographic expression of faulting in the footwall of the Wassuk Range displays steepness values consistent with a tectonically-active normal fault, regardless of segment, and our analysis of channels draining the footwall at different segment orientations display no differences that we can attribute to fundamentally different modes of slip over the geologically-recent past. Additionally, there are no patterns in long-profile data that suggest disequilibrium associated with sudden changes in fault slip. Finally, recent paleoseismic studies along the range front fault system, at the Rose Creek and Penrod Canyon alluvial fans (Fig. 2), suggest normal fault slip rates on the order of 1 mm/yr from the Late Pleistocene to the Holocene (Bormann et al., 2012; Surpless and Kroeger, 2014), far above rates of normal slip predicted by geodetic data and block modeling (e.g., Hammond et al., 2009; Bormann et al., 2016).

We are unaware of a tectonic explanation for a sudden, very recent change in strain across the Walker Lane at this latitude, so we instead propose that strain partitioning must play a role in the accommodation of recent and modern plate-boundary-related shear strain proximal to the Wassuk Range, consistent with the findings of Dong et al. (2014). Dong et al. (2014) documented a dextral strike-slip fault outboard of the Shurz segment, slipping at an estimated 1 mm/yr (Fig. 2), and Dilles (1993) indicated that a splay of the range front fault system, near the northern terminus of the range (Fig. 1), had accommodated 1.3 – 2.8 km of dextral slip since the Miocene. The trend of this fault is strike-parallel with projected dextral faults of the WLDF (Fig. 1). Because slip indicators along the Bald Mountain fault segment suggest oblique motion (Surpless, 2011), with recent slip oriented approximately N60°W on a NNW-striking fault (Fig. 2), a portion of the dextral strain is accommodated by the range front system, but not nearly enough to account for the 2 mm/yr required by geodetic data.

Thus, we suggest that more than 1 mm/yr of shear must be accommodated by dextral faults, as yet unmapped outboard of the Wassuk normal fault, and we propose that any future seismic hazard assessment of the Wassuk fault should continue to treat it as a normal fault without a significant dextral component. Although we hypothesize that significant dextral slip must be accommodated outboard of the Wassuk fault zone, we recognize the challenge of detecting strike-slip faulting within or beneath basin sediments (e.g., Dong et al., 2014), so these structures may remain undetected.

The future of the Walker Lane

The orientation of geodetically-determined shear is consistent with the proposed long-term clockwise rotation of extensional strain axes from the Pliocene to the present (e.g., Surpless, 2011), perhaps indicating a long-term shift from the dominance of Basin and Range extension to dextral deformation associated with the North American-Pacific plate boundary. In a dextral, non-coaxial strain field, extension can take place and would be expected to be oriented similar to that documented along the Bald Mountain segment. However, the dominance of a dextral strain field over long time scales would be more efficiently accommodated by dextral strike –slip faults instead of accommodated by more complex vertical-axis block rotations, pre-existing normal faults, and strain partitioning. The segmentation of the Wassuk fault zone, with several segments and two cross-range faults (the BBSF and PCF; Figs. 2 and 8A) optimally oriented to accommodate plate-boundary parallel strain, might provide

pathways for the future propagation of dextral deformation toward the northwest, utilizing these segments and accommodation structures and effectively permitting the westward migration of dextral deformation.

This westward migration would be consistent with the evolution of the White Mountain fault at the north end of the East California Shear Zone (Fig. 1), where Stockli et al. (2003) showed a westward migration of dextral slip at ca. 3 Ma from the east side of the range to the west side of the range, which had previously only accommodated normal dip-slip displacement. If future westward migration of dextral deformation similarly affects the central Walker Lane over time, possibly using pre-existing normal faults and accommodation zones, a more continuous Walker Lane, without large right- and left-stepovers of dextral deformation between the southern, central, and northern Walker Lane (Fig. 1), would permit a more efficient accommodation of plate-parallel strain. In the future, the dextral faults in the ECSZ (Fig. 1), new dextral faults in the central Walker Lane, and dextral faults of the northern Walker Lane (the Pyramid Lake fault, the Warm Springs fault, and the Mohawk fault) might link, permitting the development of a major, through-going strike-slip fault that might take up a greater percentage of total plate-boundary slip. This would be consistent with the work of Faulds et al. (2005), who suggest that the overall structure from south to north, the northward decrease in cumulative dextral displacement, and the northward decrease in the timing of strike-slip initiation portend a more efficient future Walker Lane.

CONCLUSIONS

Our findings, suggesting that Wassuk Range geomorphic evolution has been controlled by six primary fault segments, are broadly consistent with previous geologic studies of the range front fault system (Demsey, 1987; Krugh, 2008; Gorynski et al., 2013; Surpless and Kroeger, 2014). However, our geomorphologic analysis protocol, which expands on the methods of previous researchers worldwide (e.g., Whipple, 2004; Papanikolaou et al., 2013; Boulton and Whittaker, 2014; Rossi et al., 2017; He et al., 2018), allows us to not only identify mechanically-significant segments but also to estimate the strengths of the links between them. By constraining the long-term spatial and temporal variation in the accommodation of strain by segments along the Wassuk fault, we provide first-order hazard analysis, because these segments and their links fundamentally control rupture propagation during major earthquakes. These results also permit future researchers to target localities for detailed paleoseismic investigations of the Wassuk fault zone.

We also propose that strain partitioning plays a role in the accommodation of recent and modern plate-boundary-related shear strain, with Basin and Range-related normal faulting accommodated by the Wassuk fault and dextral strain likely accommodated by dextral strike-slip faults outboard (east) of the segmented fault. In addition, we suggest that continued dextral strain will eventually result in dextral faulting that migrates westward, dissecting the Wassuk Range along existing accommodation structures and more efficiently accommodating plate-boundary shear.

ACKNOWLEDGEMENTS

Funding was provided by the Geosciences Department at Trinity University, including funding from the Roy and Tinker Funds to support undergraduate student research. We are grateful for the insightful review of an early version of this manuscript by Sarah Boulton, David Ferrill, and Phillip Resor. We thank Mike Bentz, who as an undergraduate performed reconnaissance work addressing geomorphic analysis of the Wassuk Range. We also thank Kelin Whipple, who generously offered advice in our initial research efforts.

REFERENCES CITED

Aki, K., 1979, Characterization of barriers on an earthquake fault: Journal of Geophysical Research, v. 84, p. 6140–6148.

Aki, K., 1984, Asperities, barriers, and characteristic earthquakes: Journal of Geophysical Research, v. 89, p. 5867–5872.

Argus, D.F., and Gordon, R.G., 1991, Current Sierra Nevada– North America motion from very long baseline interfer-ometry—Implications for the kinematics of the western United States: Geology, v. 19, p. 1085–1088.

Benedetti, L., Manighetti, I., Gaudemer, Y., Finkel, R., Malavieille, J., Pou, K., Arnold, M., Aumaıtre, G., Bourles, D., and Keddadouche, K., 2013, Earthquake synchrony and clustering on Fucino faults (Central Italy) as revealed from in situ ^{36}Cl exposure dating: Journal of Geophysical Research Solid Earth, v. 118, p. 4948–4974, doi:10.1002/jgrb.50299.

Bennett, R.A., Wernicke, B.P., Niemi, N.A., Friedrich, A.M., and Davis, J.L., 2003, Contemporary strain rates in the northern Basin and Range Province from GPS data: Tectonics, v. 22, 1008, doi: 10.1029 /2001TC001355.

Biasi, G.P. and Weldon, R.J., 2009, San Andreas fault rupture scenarios from multiple paleoseismic records—stringing pearls: Bulletin of the Seismological Society of America, v. 99, p. 471–498.

Bingler, E.C., 1978, Geologic map of the Shurz quadrangle: Reno, NV, Nevada Bureau of Mines and Geology Map 60.

Blakely, R.J., 1995, Potential theory in gravity and magnetic applications: Cambridge University Press, Cambridge University, 441 p.

Bookhagen, B., and Strecker, M.R., 2012, Spatiotemporal trends in erosion rates across a pronounced rainfall gradient: examples from the southern central Andes: Earth and Planetary Science Letters, v. 327–328, p. 97–110.

Bormann, J.M., Surpless, B.E., Caffee, M.W., and Wesnousky, S.G., 2012, Holocene Earthquakes and Late Pleistocene Slip-Rate Estimates on the Wassuk Range Fault Zone, Nevada: Bulletin of the Seismological Society of America, v. 102, p. 1884 – 1891.

Bormann, J., Hammond, W.C., Kreemer, C., and Blewitt, G., 2016, Accommodation of missing shear in the Central Walker Lane, western North America: Constraints from dense GPS measurements: Earth and Planetary Science Letters, v.440, p. 169-177.

Boulton, S.J., and Whittaker, A.C., 2009, Quantifying the slip rates, spatial distribution and evolution of active normal faults from geomorphic analysis: field examples from an oblique-extensional graben, southern Turkey: Geomorphology, v. 104, p. 299–316.

Boulton, S., Stokes, M., and Mather, A., 2014, Transient fluvial incision as an indicator of active faulting and Plio-Quaternary uplift of the Morrocan High Atlas: Tectonophysics, v. 633, p. 16 – 33.

Burbank, D.W., and Anderson, R.S., 2012, Tectonic Geomorphology: Wiley-Blackwell Publishing, West Sussex, U.K. 454 pp.Burchfiel, B.C., Cowan, D.S., and Davis, G.A., 1992, Tectonic overview of the Cordilleran orogen in the western United States, in Buchfi el, B.C., Lipman, P.W., and Zoback, M.L., eds., The Cordilleran Orogen; Conterminous United States: Boulder, Colorado, Geological Society of America, Geology of North America, v. G3, p. 407–479.

Busby, C.J., Putirka, K., Melosh, B., Renne, P.R., Hagan, J.C., Gambs, M., and Wesoloski, C., 2018, A tale of two Walker Lane pull-apart basins in the ancestral Cascades arc, central Sierra Nevada, California: Geosphere, v. 14, p. 2068–2117.

Cashman, P., Trexler, J., Muntean, T., Faulds, J., Louie, J., and Oppliger, G., 2009, Neogene tectonic evolution of the Sierra Nevada-Basin and Range transition zone at the latitude of Carson City, Nevada. *In*: Oldow, J.S. and Cashman, P. (eds), Late Cenozoic Structure and Evolution of the Great Basin – Sierra Nevada Transition.

Castillo, M., Bishop, P., and Jansen, J.D., 2013, Knickpoint retreat and transient bedrock channel morphology triggered by base-level fall in small bedrock river catchments: the case of the Isle of Jura, Scotland: Geomorphology v. 180–181, p. 1–9.

Champagnac, J.D., Molnar, P., Sue, C., and Herman, F., 2012, Tectonics, climate, and mountain topography: Journal of Geophysical Research, v. 117, B02403.

Cowie, P.A., and Scholz, C.H., 1992, Displacement-length scaling relationship for faults: Data synthesis and discussion: Journal of Structural Geology: v. 14, p. 1149–1156, doi:10.1016/0191-8141 (92)90066-6.

Cowie, P.A., Attal, M., Tucker, G.E., Whittaker, A.C., Naylor, M., Ganas, A., Roberts, and G.P., 2006, Investigating the surface process response to fault interaction and linkage using a numerical modelling approach: Basin Research, v. 18, p. 231–266.

Crone, A.J., Machette, M.N., Bonilla, M.G., Lienkaemper, J.J., Pierce, K.L., Scott, W.E., and Bucknam, R.C., 1987, Surface faulting accompanying the Borah Peak earthquake and segmentation of the Lost River fault, central Idaho: Bulletin of the Seismological Society of America, v. 77, p. 739–770.

Crone, A., and Haller, K., 1991, Segmentation and the cosiesmic behavior of Basin and Range normal faults: examples from east-central Idaho and southwestern Montana, U.S.A.: Journal of Structural Geology, v. 13, p. 151 – 164.

Crosby, B.T., and Whipple, K.X., 2006, Knickpoint initiation and distribution within fluvial networks, 236 waterfalls in the Waipaoa River, North Island, New Zealand: Geomorphology, v. 82, p. 16–38.

Cyr, A.J., and Granger, D.E., 2008, Dynamic equilibrium among erosion, river incision, and coastal uplift in the northern and central Apennines, Italy: Geology, v. 36, p. 103–106, doi: 10.1130/G24003A.1.

D'Arcy, M., and Whittaker, A.C., 2014, Geomorphic constraints on landscape sensitivity to climate in tectonically active areas: Geomorphology, v. 204, p. 366–381.

Dawers, N.H., Anders, M.H., and Scholz, C.H., 1993, Growth of normal faults: Displacement-length scaling: Geology, v. 21, p. 1107–1110.

Dawers, N.H., and Anders, M.H., 1995, Displacement-length scaling and fault linkage: Journal of Structural Geology: v. 17, p. 607–614, doi: 10.1016/01918141(94)00091-D.

de Joussineau, G., and Aydin, A., 2009, Segmentation of strike-slip faults revisited: Pure and Applied Geophysics, v. 166), p. 1575–1594, doi:10.1007/s00024-009-0511-4.

DeLano, K., Lee, J., Roper, R., and Calvert, A., 2019, Dextral, normal, and sinistral faulting across the eastern California shear zone–Mina deflection transition, California-Nevada, USA: Geosphere, v. 15, https://doi.org/10.1130/GES01636.1.

Demsey, K., 1987, Holocene faulting and tectonic geomorphology along the Wassuk Range, west-central Nevada [MS Thesis]: Tucson, University of Arizona, 64 p.

Densmore, A.L., Dawers, N.H., Gupta, S., Guidon, R., and Goldin, T., 2004, Footwall topographic development during continental extension: Journal of Geophysical Research, v. 109, F03001, doi: 10.1029/2003JF000115.

Densmore, A.L., Hetzel, R., Ivy-Ochs, S., Krugh, W., Dawers, N., and Kubik, P., 2009, Spatial variations in catchment-averaged denudation rates from normal fault footwalls: Geology, v. 37, p. 1139-1142.

dePolo, C.M., Clark, D.G., Slemmons, D.B., and Ramelli, A.R., 1991, Historical surface faulting in the Basin and Range province, western North America: implications for fault segmentation: Journal of Structural Geology, v. 13, 123-136.

dePolo, C., and Anderson, J., 2000, Estimating the slip rates of normal faults in the Great Basin, USA: Basin Research, v. 12, p. 227 – 240.

DiBiase, R.A., Whipple, K.X., Heimsath, A.M., and Ouimet, W.B., 2009, Landscape form and millennial erosion rates in the San Gabriel Mountains, California: Earth and Planetary Science Letters, v. 289, p. 134–144.

Dilles, J. H., 1993, Cenozoic and normal and strike-slip faults in the northern Wassuk Range, western Nevada, *in* Craig, S.D., ed., Structure, tectonics, and mineralization of the Walker Lane, Walker Lane Symposium Proceedings: Reno, NV, Geological Society of Nevada, p. 114-136.

Dong, S., Ucarkus, G., Wesnousky, S., Maloney, J., Kent, G., Driscoll, N., and Baskin, R., 2014, Strike-slip faulting along the Wassuk Range of the northern Walker Lane, Nevada: Geosphere, v. 10, p. 40–48, doi: 10.1130 /GES00912.1.

DuRoss, C. B., Personius, S. F., Crone, A. J., Olig, S. S., Hylland, M. D., Lund, W. R., and Schwartz, D. P., 2016, Fault segmentation: New concepts from the Wasatch Fault Zone, Utah, USA: Journal of Geophysical Research: Solid Earth, v. 121, no. 2, p. 1131-1157.

Elliott, A.J., Oskin, M.E., Liu-Zeng, J., and Shao, Y., 2015, Rupture termination at restraining bends—the last great earthquake on the Altyn Tagh fault: Geophysical Research Letters, v. 42, no. 7, p. 2164–2170, doi:10.1002/2015GL063107.

Ellis, M. A., and Dunlap, W., 1988, Displacement variation along thrust faults: Implications for the development of large faults: Journal of Structural Geology, v. 10, p. 183–192.

Ellis, M.A., Densmore, A.L., and Anderson, R.S., 1999, Development of mountainous topography in the Basin and Ranges, USA: Basin Research, v. 11, p. 21 – 41.

Faulds, J.E., and Varga, R.J., 1998, The role of accommodation zones and transfer zones in the regional segmentation of extended terranes: J.E. Faulds and J.H. Stewart, Eds., Geological Society of America Special Paper 323, doi: 10.1130/SPE323.

Faulds, J.E., Henry, C., and Hinz, N., 2005, Kinematics of the northern Walker Lane: An incipient transform fault along the Pacific–North American plate boundary: Geology, v. 33, p. 505-508.

Ferrill, D. A., Stamatakos, J., and Sims, D., 1999, Normal fault corrugation: Implications for growth and seismicity of active normal faults: Journal of Structural Geology, v. 21, p. 1027–1038.

Field, E. H., Arrowsmith, R. J., Biasi, G. P., Bird, P., Dawson, T. E., Felzer, K. R., Jackson, D. D., Johnson, K. M., Jordan, T. H., Madden, C., Michael, A. J., Milner, K. R., Page, M. T., Parsons, T., Powers, P. M., Shaw, B. E., Thatcher, W. R., Weldon, R. J., and Zeng, Y., 2014, Uniform California Earthquake Rupture Forecast, Version 3 (UCERF3)--The Time-Independent Model: Bulletin of the Seismological Society of America, v. 104, no. 3, p. 1122-1180.

Gibson, J.R., Walsh, J.J., and Watterson, J., 1989, Modeling of bed contours and cross-sections adjacent to planar normal faults: Journal of Structural Geology, v. 11, p. 317-328.

Gilbert, C.M., and Reynolds, D.R., 1973, Character and chronology of Basin development, western margin of the Basin and Range Province: Geological Society of America Bulletin, v. 84, p. 2489-2509.

Godard, V., Bourlès, D.L., Spinabella, F., Burbank, D.W., Bookhagen, B., Fisher, G.B., Moulin, A., and Léanni, L., 2014, Dominance of tectonics over climate in Himalayan denudation: Geology, v. 42, p. 243–246.

Goldsworthy, M., and Jackson, J., 2000, Active normal fault evolution in Greece revealed by geomorphology and drainage patterns: Journal of the Geological Society of London, v. 157, p. 967-981.

Gorynski, K., Stockli, D.F., and Walker, J.D., 2013, Thermochronometrically constrained anatomy and evolution of a Miocene extensional accommodation zone and tilt domain boundary: The southern Wassuk Range, Nevada: Tectonics, v. 32, p. 516 – 539; doi: 10.1002/tect.20044.

Hammond, W.C., Kreemer, C., and Blewitt, G., 2009, Geodetic constraints on contemporary deformation in the northern Walker Lane: 3. Postseismic relaxation in the Central Nevada Seismic Belt, *In*: Oldow, J.S., Cashman, P., Eds., Late Cenozoic Structure and Evolution of the Great Basin–Sierra Nevada Transition: Geological Society of America Special Paper 447, pp. 33–54.

Hammond, W.C., Blewitt, G., and Kreemer, C., 2011, Block modeling of crustal deformation of the northern Walker Lane and Basin and Range from GPS velocities: Journal of Geophysical Research, v. 116, B04402.

Harkins, N., Kirby, E., Heimsath, A., Robinson, R., and Reiser, U., 2007, Transient fluvial incision in the head-waters of the Yellow River, northeastern Tibet, China: Journal of Geophysical Research–Earth Surface, v. 112, p. F03S04, doi:10.1029/2006JF000570.

Hasbargen, L.E., and Paola, C., 2000, Landscape instability in an experimental drainage basin: Geology, v. 28, p. 1067–1070.

He, C., Cheng, Y, Rao, G., Chen, P., Hu, J., Yu, Y., and Yao, Q., 2018, Geomorphic signatures of the evolution of active normal faults along the Langshan Mountains, North China: Geodinamica Acta, v. 30, p. 163-182.

Hecker, S., Abrahamson, N.A., and Wooddell, K.E., 2013, Variability of displacement at a point—implications for earthquake-size distribution and rupture hazard on faults: Bulletin of the Seismological Society of America, v. 103, p. 651–674.

Hijmans, R.J., Cameron, S.E., Parra, J.L., Jones, P.G., and Jarvis, A., 2005, Very high resolution interpolated climate surfaces for global land areas: International Journal of Climatology, v. 25, p. 1965–1978.

Hoeft, J.S., and Frankel, K.L., 2010, Temporal variations in extension rate along the Lone Mountain fault and strain partitioning in the Eastern California shear zone–Walker Lane: Geosphere, v. 6, p. 917–936, doi: 10 .1130 /GES00603.1.

Ichinose, G.A., Smith, K.D., Anderson, J.G., 1998, Moment tensor solutions of the 1994 to 1996 Double Spring Flat, Nevada, earthquake sequence and implications for local tectonic models: Bulletin of the Seismological Society of America, v. 88, p. 1363 – 1378.

John, D.A., 1983, Map showing distribution, ages, and petrographic characteristics of Mesozoic plutonic rocks in the Walker Lake 1 degree by 2 degree quadrangle, California and Nevada: U.S. Geological Survey Miscellaneous Field Investigations map MF-1382-B.

Kent, G.M., Babcock, J.M., Driscoll, N.W., Harding, A.J., Dingler, J.A., Seitz, G.G., Gardner, J.V., Mayer, L.A., Goldman, C.R., Heyvaert, A.C., Richards, R.C., Karlin, R., Morgan, C.W., Gayes, P.T., and Owen, L.A., 2005, 60 k.y. record of extension across the western boundary of the Basin and Range Province: Estimate of slip rates from offset shoreline terraces and a catastrophic slide beneath Lake Tahoe: Geology, v. 33, p. 365-368.

Kirby, E., Whipple, K., Burchfiel, B., Tang, W., Berger, G., Sun, Z., and Chen, Z., 2000, Neotectonics of the Min Shan, China: Implications for mechanisms driving Quaternary deformation along the eastern margin of the Tibetan Plateau: Geological Society of America Bulletin, v. 112, p. 375 – 393.

Kirby, E., and Whipple, K., 2001, Quantifying differential rock-uplift rates via stream profile analysis: Geology, v. 29, p. 415–418.

Kirby, E., and Whipple, K.X., 2012, Expression of active tectonics in erosional landscapes: Journal of Structural Geology, v. 44, p. 54–75.

Kirby, E., Whipple, K., Tang, W., and Chen, Z., 2003, Distribution of active rock uplift along the eastern margin of the Tibetan Plateau: Inferences from bedrock channel longitudinal profiles: Journal of Geophysical Research, doi:10.1029/2001JB000861

Klinger, M., 2005, Structural Characteristics and U-Pb geochronological constraints of the Pine Nut fault, Wassuk Range, west-central Nevada [unpublished M.S. Thesis]: Moscow, University of Idaho.

Klinger, Y., Etchebes, M., Tapponnier, P., and Narteau, C., 2011, Characteristic slip for five great earthquakes along the Fuyun fault in China: Nature Geoscience, v. 4, p. 389–392.

Kreemer, C., Blewitt, G., and Hammond, W.C., 2009, Geodetic constraints on contemporary deformation in the northern Walker Lane: 2. Velocity and tensor strain rate analysis, *in* Oldow, J., and Cashman, P., eds., Late Cenozoic Structure and Evolution of the Great Basin–Sierra Nevada Transition: Geological Society of America Special Paper 447, p. 33–54.

Krugh, W.K., 2008, Low-temperature thermochronologic constraints on fault array evolution and patterns of range-scale denudation [Ph.D. thesis]: Switzerland, ETH Zurich, 94 p.

Lancaster, S.T., Bras, R.L., 2002, A simple model of river meandering and its comparison to natural channels: Hydrological Processes, v. 16, p. 1–26.

Lee, J., Garwood, J., Stockli, D., and Gosse, J., 2009, Quaternary faulting in Queen Valley, California-Nevada: Implications for kinematics of fault-slip transfer in the eastern California shear zone - Walker Lane belt: v. 121, p. 599–614, doi: 10.1130/B26352.1

Leopold, L.B., Wolman, M.G., and Miller, J.P., 1964, Fluvial processes in geomorphology: Freeman, San Francisco, 511 pp.

Lopes, T.J., and Medina, R.L., 2007, Precipitation Zones of West-Central Nevada: Journal of Nevada Water Resources Association, v. 4, no 2, p. 21.

Manighetti, I., Campillo, M., Bouley, S., and Cotton, F., 2007, Earthquake scaling, fault segmentation, and structural maturity: Earth and Planetary Science Letters, v. 253, no. 3-4, p. 429-438.

Manighetti, I., Zigone, D., Campillo, M., and Cotton, F., 2009, Self-similarity of the largest-scale segmentation of the faults: Implications for earthquake behavior: Earth and Planetary Science Letters., v. 288, p. 370–381.

Manighetti, I., Caulet, C., De Barros, L., Perrin, C., Cappa, F., and Gaudemer, Y., 2015, Generic along-strike segmentation of Afar normal faults, East Africa: Implications on fault growth and stress heterogeneity on seismogenic fault planes: Geochemistry, Geophysics, Geosystems, v. 16, no. 2, p. 443-467.

Mansfield, C., and Cartwright, J.A., 2001, Fault growth by linkage: observations and implications from analogue models: Journal of Structural Geology, v. 23, p. 745-763.

Masiha, L., and Smylie, D.E., 1971, The displacement fields of inclined faults: Bulletin of the Seismological Society of America, v. 61, p. 1433-1440.

McIntyre, J., 1990, Late Cenozoic structure of the Central Wassuk Range, Mineral County, Nevada [unpublished MS thesis]: Corvallis, Oregon State University.

McLeod, A. E., Dawers, N., and Underhill, J., 2000, The propagation and linkage of normal faults: Insights from the Strathspey-Brent-Statfjord fault array, northern North Sea: Basin Research, v. 12, p. 263–284.

Miller, T.K., 1988, An analysis of the relation between stream channel sinuosity and stream channel gradient: Computers, Environment, and Urban Systems, v. 12, p. 197–207.

Miller, S.R., Baldwin, S.L., Fitzgerald, P.G., 2012. Transient fluvial incision and active surface uplift in the Woodlark Rift of eastern Papua New Guinea. Lithosphere 4, 131–149.

Oldow, J.S., Balley, A.W., Ave Lallemant, H.G., and Leeman, W.P., 1989, Phanerozoic evolution of the North American Cordillera (United States and Canada), in Bally, A.W., and Palmer, A.R., eds., The Geology of North America: An Overview: Boulder, Colorado, Geological Society of America, Geology of North America, v. A, p. 139–232.

Oldow, J.S., Aiken, C.L.V., Ferguson, J.F., Hare, J.L., and Hardyman, R.F., 2001, Active displacement transfer and differential motion between tectonic blocks within the central Walker Lane, western Great Basin: Geology, v. 29, p. 19–22.

Oldow, J.S., Geissman, J.W., and Stockli, D.F., 2008, Evolution and strain reorganization within late Neogene structural stepovers linking the central Walker Lane and northern Eastern California shear zone, western Great Basin: International Geology Review, v. 50, p. 270–290.

Papanikolaou, I., Roberts, G., Deligiannakis, G., Sakellariou, A., and Vassilakis, E., 2013, The Sparta Fault, Southern Greece: From segmentation and tectonic geomorphology to seismic hazard mapping and time dependent probabilities: Tectonophysics, v. 597, p. 85 – 105.

Patton, J., 2020, Earthquake Report: Mina Deflection in Nevada: http://earthjay.com/?p=9503 (accessed May, 2020).

Peacock, D. C. P., 1991, Displacements and segment linkage in strike-slip fault zones: Journal of Structural Geology, v. 13, p. 1025–1035.

Peacock, D.C.P., 2002, Propagation, interaction and linkage in normal fault systems: Earth-Science Reviews, v. 58, p. 121 – 142.

Petronis, M.S., Geissman, J.W., Oldow, J.S., and McIntosh, W.C., 2007, Tectonism of the southernSilver Peak Range: Paleomagnetic and geochronologic data bearing on the Neogene development of a regional extensional complex, central Walker Lane, Nevada, *in* Till, A.B., Roeske, S.M., Sample, J.C., and Foster, D.A., eds., Exhumation Associated with Continental Strike-Slip Fault Systems: Geological Society of America Special Paper 434, p. 81–106.

Prema, R., Pandey, D., and Mahender, K., 2018, Longitudinal profiling and elevation-relief analysis of the Indus: Arabian Journal of Geosciences, v. 11, doi.org/10.1007/s12517-018-3657-5.

Ramelli, A.R., Bell, J.W., dePolo, C.M. and Yount, J.C., 1999, Large-magnitude, Late Holocene earthquakes on the Genoa fault, west-central Nevada and eastern California: Bull. Seismological Soc. America, v. 89, no. 6, p. 1458-1472.

Rossi, M., Quigley, M., Fletcher, J., Whipple, K., Diaz-Torres, J.J., Seiler, C., Fifield, L.K., and Heimsath, A.M., 2017, Along-strike variation in catchment morphology and cosmogenic denudation rates reveal the pattern and history of footwall uplift, Main Gulf Escarpment, Baja California: Geological Society of America Bulletin, v. 129, p. 837 – 854.

Sagy, A., Brodsky, E., and Axen, G., 2007, Evolution of fault-surface roughness with slip: Geology, v. 35, p. 283–286.

Saltus, R.W., 1988, Bouguer gravity anomaly map of Nevada: Nevada Bureau of Mines and Geology, Map 94A, scale 1:750,000.

Savage, J.C., and Hastie, L.M., 1966, Surface deformation associated with dip-slip faulting: Journal of Geophysical Research, v. 71, p. 4897-4904.

Scharer, K., Weldon, R., II, Streig, A., and Fumal, T., 2014, Paleoearthquakes at Frazier Mountain, California delimit extent and frequency of past San Andreas Fault ruptures along 1857 trace: Geophysical Research Letters, v. 41, p. 4527–4534.

Schumm, S.A., and Khan, H.R., 1972, Experimental study of channel patterns: Geological Society of America Bulletin, v. 83, p. 1755—1770.

Schwartz, D. P., and Coppersmith, K. J., 1984, Fault behavior and characteristic earthquakes: Examples from the Wasatch and San Andreas fault zones: Journal of Geophysical Research, v. 89, p. 5681-5698.

Schwartz, D.P., Haeussler, P.J., Seitz, G.G., and Dawson, T.E., 2012, Why the 2002 Denali fault rupture propagated onto the Totschunda fault—implications for fault branching and seismic hazards: Journal of Geophysical Research, v. 117, B11304, doi:10.1029/2011JB008918.

Schweickert, R.A., Lahren, M.M., Smith, K.D., Howle, J.F., and Ichinose, G, 2004, Transtensional deformation in the Lake Tahoe region, California and Nevada, USA: Tectonophysics, v. 392, p. 303–323.

Segall, P., and Pollard, D., 1980, Mechanics of discontinuous faults: Journal of Geophysical Research, v. 85, p. 4337–4350.

Sibson, R. H., 1986, Earthquakes and rock deformation in crustal fault zones: Annual Review of Earth and Planetary Sciences, v. 14, p. 149 - 175.

Soliva, R., and Benedicto, A., 2004, A linkage criterion for segmented normal faults: Journal of Structural Geology, v. 26, p. 2251–2267.

Snyder, N.P., Whipple, K.X., Tucker, G.E., Merrits, D.J., 2000, Landscape evolution to tectonic forcing: digital elevation model analysis of stream profiles in the Mendocino triple junction region, northern California: Geological Society of America Bulletin, v. 112, p. 1250–1263.

Stewart, J.H., and Dohrenwend, J.H., 1981, Geologic map of the Mount Grant quadrangle, Lyon and Mineral Counties, Nevada with surficial geology: Boulder, United States Geological Survey Miscellaneous Field Studies Map MF-1278.

Stewart, J.H., 1988, Tectonics of the Walker Lane belt, west ern Great Basin—Mesozoic and Cenozoic deformation in a zone of shear, *in* Ernst, W.G., ed., Metamorphism and Crustal Evolution of the Western United States: Upper Saddle River, New Jersey, Prentice Hall, Rubey Volume VII, p. 683–713.

Stewart, M., and Taylor, W., 1996, Structural analysis and fault segment boundary identification along the Hurricane fault in southwestern Utah: Journal of Structural Geology, v. 18, p. 1017 – 1029.

Stockli, D. F., Surpless, B. E., and Dumitru, T. A., 2002, Thermochronological constraints on the timing and magnitude of Miocene and Pliocene extension in the central Wassuk Range, western Nevada: Tectonics, v. 21, doi: 10.1029/2001TC001295.

Stockli, D.F., Dumitru, T., McWilliams, M., and Farley, K., 2003, Cenozoic tectonic evolution of the White Mountains, California and Nevada: Geological Society of America Bulletin, v. 115, p. 788-816.

Surpless, B.E., Stockli, D.F., Dumitru, T.A., and Miller, E.L., 2002, Two phase westward encroachment of Basin and Range extension into the northern Sierra Nevada. Tectonics, vol. 21, 1, 10.1029/2000TC001257.

Surpless, B.E., 2008, Modern strain localization in the central Walker Lane, western United States: Implications for the evolution of intraplate deformation in transtensional settings: Tectonophysics, v. 457, p. 239–253.

Surpless, B.E., 2010, Geologic Map of the Central Wassuk Range, western Nevada: Geological Society of America Map and Chart Series MCH098, scale 1:24000 DOI: 10.1130/2010.MCH098.

Surpless, B.E., 2011, Cenozoic tectonic evolution of the central Wassuk Range, western Nevada, USA: International Geology Review, v. 54, p. 547 – 571, DOI: 10.1080/00206814.2010.548117.

Surpless, B.E., and Kroeger, G., 2014, The unusual temporal and spatial slip history of the Wassuk Range normal fault, western Nevada (USA): implications for seismic hazard and Walker Lane deformation: Geological Society of America Bulletin, doi: 10.1130/B31159.1.

Suter, M., 2008, Structural configuration of the Otates fault (Southern Basin and Range Province) and its rupture in the 3 May 1887 M 7.5 Sonora, Mexico, earthquake: Bulletin of the Seismological Society of America, v. 98, p. 2879–2893.

Suter, M., 2015, Rupture of the Pitáycachi Fault in the 1887 M_w 7.5 Sonora, Mexico earthquake (southern Basin-and- Range Province)—rupture kinematics and epicenter inferred from rupture branching patterns: Journal of Geophysical Research – Solid Earth, v. 120, p. 617–641.

Trudgill, B., and Cartwright, J., 1994, Relay-ramp forms and normal-fault linkages, Canyonlands National Park, Utah: Geological Society of America Bulletin, v. 106, p. 1143–1157.

Tucker, G.E., and Bras, R.L., 1998, Hillslope processes, drainage density, and landscape morphology: Water Resources Research, v. 34, p. 2751–2764.

Tucker, G.E., and Whipple, K.X., 2002, Topographic outcomes predicted by stream erosion models: sensitivity analysis and intermodel comparison: Journal of Geophysical Reseach-Solid Earth, v. 107, p. 2179-2194.

U.S. Geological Survey, 2017, 1/3rd arc-second Digital Elevation Models (DEMs) - USGS National Map 3DEP Downloadable Data Collection: U.S. Geological Survey.

U.S. Geological Survey, 2020a, M 5.2 - 30km SE of Bodie, CA: https://earthquake.usgs.gov/earthquakes/eventpage/nc73367270/executive (accessed May, 2020).

U.S. Geological Survey, 2020b, M 6.5 - 65 km W of Tonopah, Nevada: https://earthquake.usgs.gov/earthquakes/eventpage/nn00725272/executive (accessed May, 2020).

Wallace, R.E., 1984, Fault scarps formed during the earthquakes of October 2, 1915, in Pleasant Valley, Nevada, and some tectonic implications: U.S. Geological Survey Professional Paper 1274-A, 32 p.

Walsh, J.J., and Watterson, J., 1991, Geometric and kinematic coherence and scale effects in normal fault systems, *in* Roberts, A.M., Yielding, G., Freeman, B., eds. The Geometry of Normal Faults: Geological Society Special Publication, v. 56, p. 193-203.

Wei, Z., Bi, L., Xu, Y., and He, H., 2015, Evaluating knickpoint recession along an active fault for paleoseismological analysis: The Huoshan Piedmont, Eastern China: Geomorphology, v. 235, p. 63 – 76.

Wells, D.L., 2013, Updated empirical relationships among magnitude, rupture area, rupture length, and surface displacement [abs.]: Seismological Research Letters, v. 84, p. 309.

Wells, D.L., and Coppersmith, K.J., 1994, New empirical relationships among magnitude, rupture length, rupture width, rupture area, and surface displacement: Bulletin of the Seismological Society of America, v. 84, p. 974–1002.

Wernicke, B., 1992, Cenozoic extensional tectonics of the U.S. Cordillera, *in* Burchfiel, B. C., Lipman, P. W., and Zoback, M. L, eds., The Cordilleran Orogen: Conterminous U.S.: Boulder, Colorado, Geological Society of America, The Geology of North America, v. G-3.

Wesnousky, S. G., 1988, Seismological and structural evolution of strike-slip faults: Nature, v. 335, p. 340–343, doi: 10.1038/335340a0.

Wesnousky, S.G., 2005, Active faulting in the Walker Lane: Tectonics, v. 24, TC3009, doi: 10.1029/2004TC001645.

Wesnousky, S. G., 2006, Predicting the endpoints of earthquake ruptures: Nature, v. 444, no. 7117, p. 358-360.

Wesnousky, S. G., 2008, Displacement and geometrical characteristics of earthquake surface ruptures: Issues and implications for seismic-hazard analysis and the process of earthquake rupture: Bulletin of the Seismological Society of America, v. 98, no. 4, p. 1609-1632.

Whipple, K.X., Tucker, G.E., 1999, Dynamics of the stream power incision model: implications for the height limits of mountain ranges, landscape response timescales and research needs: Journal of Geophysical Research, v. 104, p. 17661–17674.

Whipple, K. X., and Tucker, G., 2002, Implications of sediment-flux-dependent river incision models for landscape evolution: Journal of Geophysical Research, v. 107; doi:10.1029/2000JB000044.

Whipple, K., 2004, Bedrock rivers and the geomorphology of active orogens: Annual Reviews of Earth and Planetary Sciences, v. 32, p. 151 – 185; doi: 10.1146/annurev.earth.32.101802.120356

Whipple, K., Wobus, C., Crosby, B., Kirby, E., and Sheehan, D., 2007, New Tools for Quantitative Geomorphology: Extraction and Interpretation of Stream Profiles from Digital Topographic Data: Geological Society of America Workshop, 26 p.

Whittaker, A.C., Attal, M., Cowie, P.A., Tucker, G.E., and Roberts, G., 2008, Decoding temporal and spatial patterns of fault uplift using transient river long-profiles: Geomorphology, v. 100, p. 506–526. doi:10.1016/j.geomorph.2008.01.018.

Whittaker, A.C., 2012, How do landscapes record tectonics and climate?: Lithosphere, v. 4, p. 160–164, doi:10.1130/RF.L003.1.

Willemse, E. J. M., Pollard, D. D., and Aydin, A., 1996, Three-dimensional analyses of slip distributions on normal fault arrays with consequences for fault scaling: Journal of Structural Geology, v. 18, no. 2-3, p. 295-309.

Wobus, C., Hodges, K.V., and Whipple, K.X., 2003, Has focused denudation sustained active thrusting at the Himalayan topographic front?: Geology, v. 31, p. 861–864, doi:10.1130/G19730.1.

Wobus, C.W., Whipple, K.X., Kirby, E., Snyder, N., Johnson, J., Spyropolou, K., Crosby, B., and Sheehan, D., 2006, Tectonics from topography: Procedures, promise, and pitfalls, in Willett, S.D., et al., eds., Tectonics, climate, and landscape evolution: Geological Society of America Special Paper 398, p. 55–74.

Wong, I., Lund, W., DuRoss, C., Thomas, P., Arabasz, W., Crone, A., Hylland, M., Luco, N., Olig, S., Pechmann, J., Personius, S., Peterse, M., Schwartz, D., Smith, R., and Bowman, S., 2016, Earthquake Probabilities for the Wasatch Front region in Utah, Idaho, and Wyoming, Utah Geological Survey Miscellaneous Publication 16-3: Salt Lake City, Utah, Utah Geological Survey, 178 p.

Wong, I., Lund, W., DuRoss, C., Thomas, P., Arabasz, W., Crone, A., Hylland, M., Luco, N., Olig, S., Pechmann, J., Personius, S., Peterse, M., Schwartz, D., Smith, R., and Bowman, S., 2017, Estimating the probabilities of future large earthquakes along the Wasatch front, *in* Lund, W., Emerman, S., Wang, W., and Zanazzi, A., Eds., Geology and Resources of the Wasatch: Back to Front: Utah Geological Association Publication 46, Salt Lake City, Utah, 19 p.

Wu, D., and Bruhn, R.L., 1994, Geometry and kinematics of active normal faults, South Oquirrh Mountains, Utah: implication for fault growth: Journal of Structural Geology, v. 16, p. 1061-1075.

Zamolyi, A., Szekely, B., Draganits, E., and Timar, G., 2010, Neotectonic control on river sinuosity at the western margin of the Little Hungarian Plain: Geomorphology, v. 122, p. 231-243.

Zhang, P., Mao, F., and Slemmons, D., 1999, Rupture terminations and size of segment boundaries from historical earthquake ruptures in the Basin and Range Province: Tectonophysics, v. 308, p. 37–52.

TABLE S1. T-TEST RESULTS FOR COMPARISON OF FOOTWALL DOMAIN DATA

	Domains compared	Shurz N - Shurz S	Shurz S - Bald Mtn. N	Bald Mtn. N - Bald Mtn. S	Bald Mtn. S - Mt. Grant	Mt. Grant - Coryville	Coryville - Luckyboy	Luckyboy - Anch. Hills
	d.f. (n - 2)	7	5	4	4	2	3	3
	95% conf. exceedance value	2.365	2.571	2.776	2.776	4.303	3.182	3.182
Calculated t values	**Relief**	1.959	***13.39***	***8.763***	***21.89***	***34.93***	***9.74***	***4.26***
	Channel Length	***4.012***	***5.502***	***2.973***	2.638	***41.49***	***66.58***	***14.56***
	Straight-line distance	2.191	***7.193***	0.133	2.083	***42.61***	***30.83***	***15.43***
	Scaled relief-length value (Z)	***3.133***	***8.024***	***8.493***	***14.77***	***55.57***	***60.89***	***14.23***
	Average Slope	***5.047***	2.503	1.733	***5.693***	***16.84***	***3.699***	0.0533
	Catchment area	***5.400***	***3.283***	2.302	2.001	***23.53***	***3.714***	0.973
	Sinuosity	***3.359***	1.458	***7.539***	1.479	***10.30***	***13.72***	0.841
	Outlet Reach k_{sn} value	***3.099***	0.159	0.088	***7.677***	***11.11***	***15.47***	***12.82***

All T-test analyses are based on the values listed in Table 1. Calculations do not integrate 2σ values. In the table above, n = total number of bedrock channels from both domains. Exceedance values (from a statistical t-table) are based on the number of degrees of freedom (d.f.) and probability (P= 0.05 or 95% confidence). A t-value (absolute value) that is greater than the 95% confidence exceedance value indicates a statistical difference between populations (shown in ***bold italics*** in above table). A t-value that is below the exceedance value indicates sample populations that are not statistically different. See Approaches and Methods for discussion of the calculation of t values.